COO-2245-38

COOLANT MIXING IN LMFBR ROD BUNDLES AND OUTLET PLENUM MIXING TRANSIENTS

Progress Report

Principal Investigators
Neil E. Todreas - Tasks I and II
Michael W. Golay - Task III
Lothar Wolf - Task IV

Massachusetts Institute of Technology
Department of Nuclear Engineering
Cambridge, Massachusetts 02139

December 1, 1976 - February 28, 1977

Prepared for the U.S. Energy Research and Development Administration under Contract No. AT(11-1)-2245

DISCLAIMER

Reports and Papers Published under MIT Coolant Mixing in LMFBR Rod Bundles Project

A. Quarterly Progress Reports (Available from National Technical Information Service, U.S. Department of Commerce, Springfield, VA 22151)

COO-2245-1	Period June 1, 1972 - November 30, 1972
COO-2245-2	Period December 1, 1972 - February 28, 1973
COO-2245-3	Period March 1, 1973 - May 31, 1973
COO-2245-6	Period June 1, 1973 - August 31, 1973
COO-2245-7	Period September 1, 1973 - November 30, 1973
COO-2245-8	Period December 1, 1973 - February 28, 1974
COO-2245-10	Period March 1, 1974 - May 31, 1974
COO-2245-13	Period June 1, 1974 - August 31, 1974
COO-2245-14	Period September 1, 1974 - November 31, 1974
COO-2245-15	Period December 1, 1974 - February 28, 1975
COO-2245-23	Period March 1, 1975 - May 31, 1975
COO-2245-25	Period June 1, 1975 - August 31, 1975
COO-2245-26	Period September 1, 1975 - November 30, 1975
COO-2245-28	Period December 1, 1975 - February 29, 1976
COO-2245-30	Period March 1, 1976 - May 31, 1976
COO-2245-31	Period June 1, 1976 - August 31, 1976
COO-2245-34	Period September 1, 1976 - November 30, 1976
COO-2245-38	Period December 1, 1976 - February 28, 1977

Reports Issued Under This Contract

B. Topical Reports (Available from National Technical Information Service, U.S. Department of Commerce, Springfield, VA 22151)

E. Khan and N. Todreas, "A Review of Recent Analytical and Experimental Studies Applicable to LMFBR Fuel and Blanket Assembly Design," COO-2245-4TR, MIT, Sept. 1973.

E. Khan, W. Rohsenow, A. Sonin and N. Todreas, "A Simplified Approach for Predicting Temperature Distribution in Wire Wrapped Assemblies," COO-2245-5TR, MIT, Sept. 1973.

T. Eaton and N. Todreas, "Instrumentation Methods for Interchannel Coolant Mixing Studies in Wire-Wrap Spaced Nuclear Fuel Assemblies," COO-2245-9TR, MIT, June 1974.

Y.B. Chen, K. Ip, N.E. Todreas, "Velocity Measurements in Edge Subchannels of Wire Wrapped LMFBR Fuel Assemblies," COO-2245-11TR, MIT, September 1974.

E. Khan, N. Todreas, W. Rohsenow, A.A. Sonin, "Analysis of Mixing Data Relevant to Wire-Wrapped Fuel Assembly Thermal-Hydraulic Design," COO-2245-12TR, MIT, September 1974.

E. Khan, W. Rohsenow, A. Sonin, N. Todreas, "A Porous Body Model for Predicting Temperature Distributions in Wire Wrapped Fuel and Blanket Assemblies of a LMFBR," COO-2245-16TR, MIT, March 1975.

E. Khan, W.M. Rohsenow, A. Sonin, N. Todreas, "Input Parameters to the ENERGY Code (To be used with the ENERGY Code Manual) COO-2245-17TR, MIT, May 1975.

E. Khan, W. Rohsenow, A. Sonin, N. Todreas, "Manual for ENERGY Codes I, II, III," COO-2245-18TR, MIT, May 1975.

E. Khan, W. Rohsenow, A. Sonin, N. Todreas, "Manual for ENERGY Codes I, II, III Computer Programs," COO-2245-18TR Revision 1, MIT, July 1976.

P. Carajilescov and N. Todreas, "Experimental and Analytical Study of Axial Turbulent Flows in an Interior Subchannel of a Bare Rod Bundle," COO-2245-19TR, MIT,

B. Chen and N. Todreas, "Prediction of Coolant Temperature Field in a Breeder Reactor Including Interassembly Heat Transfer," COO-2245-20TR, MIT, May 1975.

F. Carre and N. Todreas, "Development of Input Data to ENERGY Code for Analysis of Reactor Fuel Bundles," COO-2245-21TR, MIT, May 1975.

Reports Issued Under This Contract

B. Topical Reports, Continued

H. Ninokata and N.E. Todreas, "Turbulent Momentum Exchange Coefficients for Reactor Fuel Bundle Analysis," COO-2245-22TR, MIT, June 1975.

R. Anoba and N. Todreas, "Coolant Mixing in LMFBR Rod Bundles and Outlet Plenum Mixing Transients," COO-2245-24TR, August 1975.

B. Bosy, "Fabrication Details for Wire Wrapped Fuel Assembly Components," COO-2245-27TR, MIT, November 1975.

Ralph G. Bennett and Michael W. Golay, "Interferometric Investigation of Turbulently Fluctuating Temperature in an LMFBR Outlet Plenum Geometry," COO-2245-29TR, MIT, June 1976.

N.E. Todreas, "Analysis Methods for LMFBR Wire Wrapped Bundles," COO-2245-32TR, MIT, November 1976.

K.L. Basehore and N.E. Todreas, "Development of Stability Criteria and an Interassembly Conduction Model for the Thermal-Hydraulics Code SUPERENERGY," COO-2245-33TR, MIT December 1976.

Robert Masterson and Neil E. Todreas, "Analysis of the Feasibility of Implementing an Implicit Temporal Differencing Scheme in the SUPERENERGY Code," COO-2245-35TR, MIT, February 1977.

S. Glazer, C. Chiu and N. Todreas, "Collection and Evaluation of Salt Mixing Data with the Real Time Data Acquisition System," COO-2245-36TR, MIT, April 1977.

B. Mikic, E.U. Khan and N.E. Todreas "An Approximate Method for Predicting Temperature Distribution in Wire Wrapped Fuel Assemblies of a LMFBR," COO-2245-37TR, MIT, April 1977.

Reports Issued under this Contract

C. Papers and Summaries

Yi Bin Chen, Ka-Lam Ip, Neil E. Todreas, "Velocity Measurements in Edge Channels of Wire-Wrapped LMFBR Fuel Assemblies," American Nuclear Society Transactions Vol. 19, 1974, pp. 323-324.

P. Carajilescov, N. Todreas, "Experimental and Analytical Study of Axial Turbulent Flows in an Interior Subchannel of a Bare Rod Bundle," J. of Heat Transfer, Vol. 98, No. 2, May 1976, pp. 262-268 (Included as Appendix to Quarterly Progress Report, COO-2245-15).

E. Khan, W. Rohsenow, A. Sonin, N. Todreas, "A Porous Body Model for Predicting Temperature Distribution in Wire-Wrapped Fuel Rod Assemblies," Nuclear Engineering and Design, 35 (1975) 1-12.

E. Khan, W. Rohsenow, A. Sonin, N. Todreas, "A Porous Body Model for Predicting Temperature Distribution in Wire-Wrapped Rod Assemblies Operating in Combined Forced and Free Convection," Nuclear Engineering and Design, 35 (1975) 199-211.

Ralph G. Bennett and Michael W. Golay, "Development of an Optical Method for Measurement of Temperature Fluctuation in Turbulent Flows," American Nuclear Society Transactions, Vol. 22, 1975, p. 581.

B. Chen and N. Todreas, "Prediction of the Coolant Temperature Field in a Breeder Reactor Including Interassembly Heat Transfer," Nuclear Engineering and Design 35, (1975) 423-440 (Included as Appendix to Quarterly Progress Report, COO-2245-23).

R. Bennett and M.W. Golay, "Interferometric Investigation of Turbulently Fluctuating Temperature in an LMFBR Outlet Plenum Geometry," Accepted for the ASME Winter Annual Meeting, Dec., 1976, (Included as Appendix in Quarterly Progress Report, COO-2245-30).

B.B. Mikic, E.U. Khan, N.E. Todreas, "An Approximate Method for Predicting Temperature Distribution in Wire Wrapped Fuel Assemblies of a Liquid Metal Fast Breeder Reactor," Mech. Res. Comm., Vol. 3, 353-360 (1976).

Reports Issued Under this Contract

C. Papers and Summaries (Continued)

L. Wolf, R. Karimi, I.Y. Kim, C.N. Wong, M.K, Yeung "2-D Thermoelastic Analysis of LMFBR Fuel Rod Claddings," Paper C4/d,4th International Conf. Structural Mechanics in Reactor Technology, San Francisco, August 1977.

M. Yeung, L. Wolf, "Effective Conduction Mixing Lengths for Subchannel Analysis of Finite Hexagonal LMFBR Bundles," ANS Meeting, New York, June 1977.

C. Chiu and N. Todreas,"Flow Split Measurements In An LMFBR Radial Blanket Assembly," ANS Meeting, New York, June 1977.

Commencing with report COO-2245-30, a new task, TASK IV, which has been added to the contract, was reported. This TASK IV and TASK IID differ in that TASK IV is initially concentrated on thermal analyses using slug and laminar velocity profiles while TASK IID is concentrated on hydrodynamic analyses of turbulent velocity fields.

COOLANT MIXING IN LMFBR ROD BUNDLES AND OUTLET PLENUM MIXING TRANSIENTS

Contract AT(11-1)-2245

Quarterly Progress Report

The work of this contract has been divided into the following Tasks:

TASK I: BUNDLE GEOMETRY (WRAPPED AND BARE RODS)

- TASK IA: Assessment of Available Data
- TASK IB: Experimental Bundle Water Mixing Investigation
- TASK IC: Experimental Bundle Peripheral Velocity Measurements (Laser Anemometer)
- TASK ID: Analytic Model Development - Bundles

TASK II: SUBCHANNEL GEOMETRY (BARE RODS)

- TASK IIA: Assessment of Available Data
- TASK IIB: Experimental Subchannel Water Mixing Investigation
- TASK IIC: Experimental Subchannel Local Parameter Measurements (Laser Anemometer)
- TASK IID: Analytic Model Development - Subchannels

TASK III: LMFBR OUTLET PLENUM FLOW MIXING

- TASK IIIA: Analytical and Experimental Investigation of Velocity and Temperature Fields

TASK IV: THEORETICAL DETERMINATION OF LOCAL TEMPERATURE FIELDS IN LMFBR FUEL ROD BUNDLES

TASK I: BUNDLE GEOMETRY (WRAPPED AND BARE RODS)

TASK IA: Assessment of Available Data and Codes (Kerry Basehore)

No work was performed this quarter.

TASK IB.2 Experimental Bundle Water Mixing Investigation

Repeat of Laminar and Transition Flow - 61 Pin Fuel Mixing Experiments (Stuart Glazer)

During the current quarter, the bundle was disassembled several times due to broken spacer wires. All pins have finally been repaired and the bundle reassembled. In preparation for rapid flow split data collection, changes were made to the inlet flow piping and the main rotameter. The rotameter has been successfully calibrated, and flow split data collection has begun. It is currently planned to measure flow splits at Reynolds numbers of 10,000, 6,000, 4,000, 3,000 and 2,000. Particular care will be exercised in the transition regime to verify the sharp changes in flow split noted by C. Chiu and reported in [1]. Measurements will be made at additional Reynolds numbers as necessary to confirm the presence of the sudden hump.

Immediately following flow split measurements the Real Time Data Acquisition System will be used to retake salt mixing data in the 61 pin fuel bundle. Injection rods have been essentially completed, and will be ready for insertion into the bundle immediately upon completion of flow split tests. Flow split data is prerequisite for the salt mixing tests, as accurate evaluation of salt mass balances (salt measured at outlet/salt injected) cannot be made without it.

In preparation for all future salt mixing experiments, the Real Time Data Acquisition System was devised. During the past quarter, the system development was completed. Complete system details, including operating instructions, will shortly be published [2]. Accuracy of the system has been tested via salt mixing experiments on the 61 pin blanket bundle with alternating wire wrap. Preliminary test data evaluation indicates the system is highly accurate. Salt mass balances have been observed very close to 1.0 using flow split data previously taken by C. Chiu. Further evaluation of the Real Time Data Acquisition System will be made during repeat of the salt mixing experiments on the 61 pin fuel bundle, and by duplication of the reduction of data previously taken with the older hardware built for Alan Hanson for the 61 pin blanket bundle and reported in [1].

TASK IB.3 217 Pin Mixing Experiments (Stuart Glazer)

The 217 pin bundle was slightly modified to facilitate flow split testing by the isokinetic sampling technique reported in [3]. Although essentially currently ready for testing, no flow split experiments have yet been performed since the test rig is loaded with the 61 pin bundle. If considered necessary, salt mixing tests could be performed upon completion of 3 injector rods and a sufficient number of resistance probes. The Real Time Data Acquisition System does now have the capability to collect, store, and reduce data from the 438 resistance probes required (1 per subchannel).

TASK IB.4 61 Pin Blanket Bundle Experiments (Chong Chiu)

During this quarter an attempt was made to predict the WARD Thermal-Hydraulic Test results by using SUPERENERGY. The input parameters ε^*, C_1, x_1, x_2 and x_3 were obtained from the test results obtained last quarter. The analysis also explicitly assessed the uncertainties introduced by the as-built tolerance and the range of pin packing arrangements possible within this tolerance. The conclusions of this task are summarized below.

1) Experimental effort on determination of C_1 should take priority over that of ε^* due to the high inherent interior coolant temperature uncertainty due to the bundle tolerance.

2) Further study on the flow splits with respect to the variation of rod alignment modes, rather than refined code development, is recommended for reactor design application.

The prediction results and details of rod alignment mode will be available as a topical report "WARD Blanket Assembly Pre-Test Prediction by SUPERENERGY" in the near future.

Moreover, much effort was devoted to obtain the mixing data from the alternating wire wrapped bundle. A qualitative assessment report on the coolant mixing effectiveness will be made in early April. No conclusions on the effectiveness of this alternating wire bundle design versus the standard design are available at this time.

Two topical reports on the subjects of "Technology Development on the Measurement of the Subchannel Coolant Flow" and "Mixing Experiments in the LMFBR Blanket", are being written. Hopefully, they will be issued before the end of the next quarter.

TASK IC: Experimental Bundle Peripheral Velocity Measurements (Laser Anemometer)

No work was performed this quarter.

TASK ID: Analytic Model Development - Bundles

TASK ID.1 Steady State SUPERENERGY (Kerry Basehore)

1. Swirl Flow Model

Work continued this quarter on the incorporation of a variable swirl flow model into the SUPERENERGY code. The forcing function of the swirl flow is a function of the wire wrap angle and lead length. The data base and reduction methods used in the formulation of this function have been previously reported in last quarter's progress report (COO-2245-34).

Implementation of this model into the code was accomplished quite readily by normalizing the forcing function with its average value, introducing this into the code as a data set, and using a table lookup routine to find the function value with respect to the wire wrap angle of a given edge subchannel. A comparison of this new variable swirl model and the old constant swirl model was accomplished by using ORNL FFM-2A assembly data [4]. Results are presented for the bundle outlet in Figs. 2 through 5. A cross section of the FFM-2A assembly with appropriate nomenclature is presented in Fig. 1. Table 1 provides a listing of pin powers in the various tests.

The advantages of a variable swirl model over a constant model, if any exist, should appear in the prediction of a highly assymetric power profile bundle. Figures 4 and 5 represent such a profile with three neighboring peripheral pins producing the entire bundle power in the nineteen pin bundle. The profiles for each model appear similar with neither matching the data points particularly well. There are some very substantial local differences, however, with deviations of up to 25% of the total average temperature rise of 25°F occurring. This suggests that the variable swirl effects may indeed be important locally in some bundle conditions.

A topical report is soon to be released which will treat this subject in more detail and include some additional work on the effects of the variable swirl flow model on the transverse velocity correlation and the subchannel mass balance.

2. G.E. Secondary Control Assembly

Work is progressing on a computer model of the Clinch River Secondary Control Assembly which General Electric has contracted to build. The assembly is particularly hard to model due to downflow in the bundle center and variable heat flux conditions at the wall. Preliminary results indicate that the choice of a semi-analytical modeling technique is justified and that interfacing with SUPERENERGY in order to model interassembly heat transfer is possible, but as yet unproven. A detailed description of the method of solution has been outlined in a June 24, 1976 letter to Jay Lipps at General Electric. A topical report will be written next quarter.

TASK ID.2 Analytical Model Development - Transient SUPERENERGY (Stuart Glazer)

During the current quarter, research on numerical techniques for modification of the steady state SUPERENERGY code to handle transients reported in [1] was reviewed by R. Masterson of MIT. Suggestions made by Mr. Masterson indicate that a temporally implicit differencing scheme may be used in the coolant without requiring computational or core storage in excess of the fully explicit technique. A topical report [5] will be issued on these conclusions. An additional advantage of the implicit method is unconditional temporal stability. During the next quarter, development of the transient SUPERENERGY code will proceed with top prority, with the intent of integration of the program into a package of steady state and transient thermal hydraulics codes of varying capabilities by Kerry Basehore and S. Glazer.

References

[1] N. Todreas, M. Golay, L. Wolf, "Coolant Mixing in LMFBR Rod Bundles and Outlet Mixing Transients," Progress Report, COO-2245-34, November 1976.

[2] S. Glazer, C. Chiu, N. Todreas, "Collection and Evaluation of Salt Mixing Data with the Real Time Data Acquisition System," Topical Report, COO-2245-36TR.

[3] N. Todreas, M. Golay, L. Wolf, "Coolant Mixing in LMFBR Rod Bundles and Outlet Mixing Transients," Progress Report, COO-2245-31, August 1976.

[4] M.H. Fontana, R.E. MacPherson, P.A. Gnadt, L.F. Parsly and J.L. Wantland, Temperature Distribution in a 19-Rod Simulated LMFBR Fuel Assembly in a Hexagonal Duct (Fuel Failure Mockup Bundle 2A) - Record of Experimental Data, ONRL-TM-4113, Spetember 1973.

[5] R. Masterson and N.E. Todreas, "Analysis of the Feasibility of Implementing an Implicit Temporal Differencing Scheme in the SUPERENERGY Code," COO-2245-35TR, MIT, February 1977.

Table 1

ORNL FFM-2A Pin Powers

Figure Number	ORNL Identification			Pin* Numbers	Combined Power (KW)
	Series	Test	Run		
2	2	14	101	1	8.93
				8,18,19	39.33
				12,13,14	13.11
				2,7,9,17	44.25
				4,5,11,15	26.00
				3,6,10,16	34.78
3	2	9	201	1	- 0.03
				8,18,19	18.10
				12,13,14	- 0.09
				2,7,9,17	17.12
				4,5,11,15	- 0.09
				3,6,10,16	17.43
4	2	9	401	1	- 0.03
				8,18,19	0.00
				12,13,14	52.07
				2,7,9,17	- 0.04
				4,5,11,15	- 0.09
				3,6,10,16	- 0.13
4	2	9	101	1	- 0.03
				8,18,19	52.98
				12,13,14	- 0.10
				2,7,9,17	- 0.02
				4,5,11,15	- 0.09
				3,6,10,16	- 0.14

*ORNL pin numbering scheme shown on Figure 1

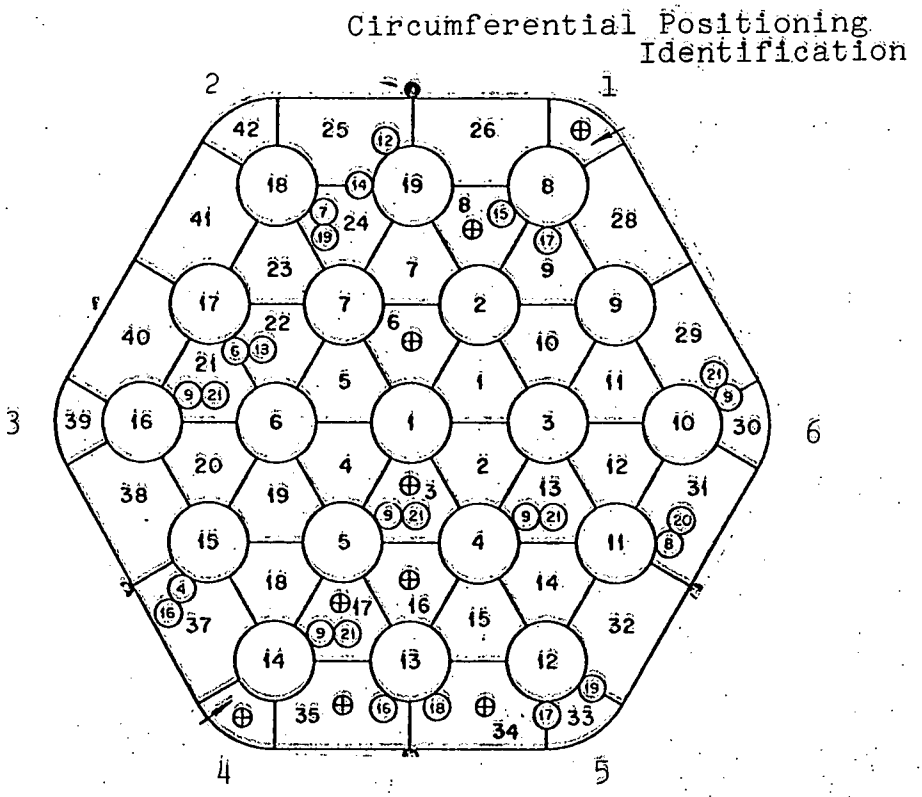

Figure 1 ORNL FFM-2A Bundle (looking upstream)

Figure 2

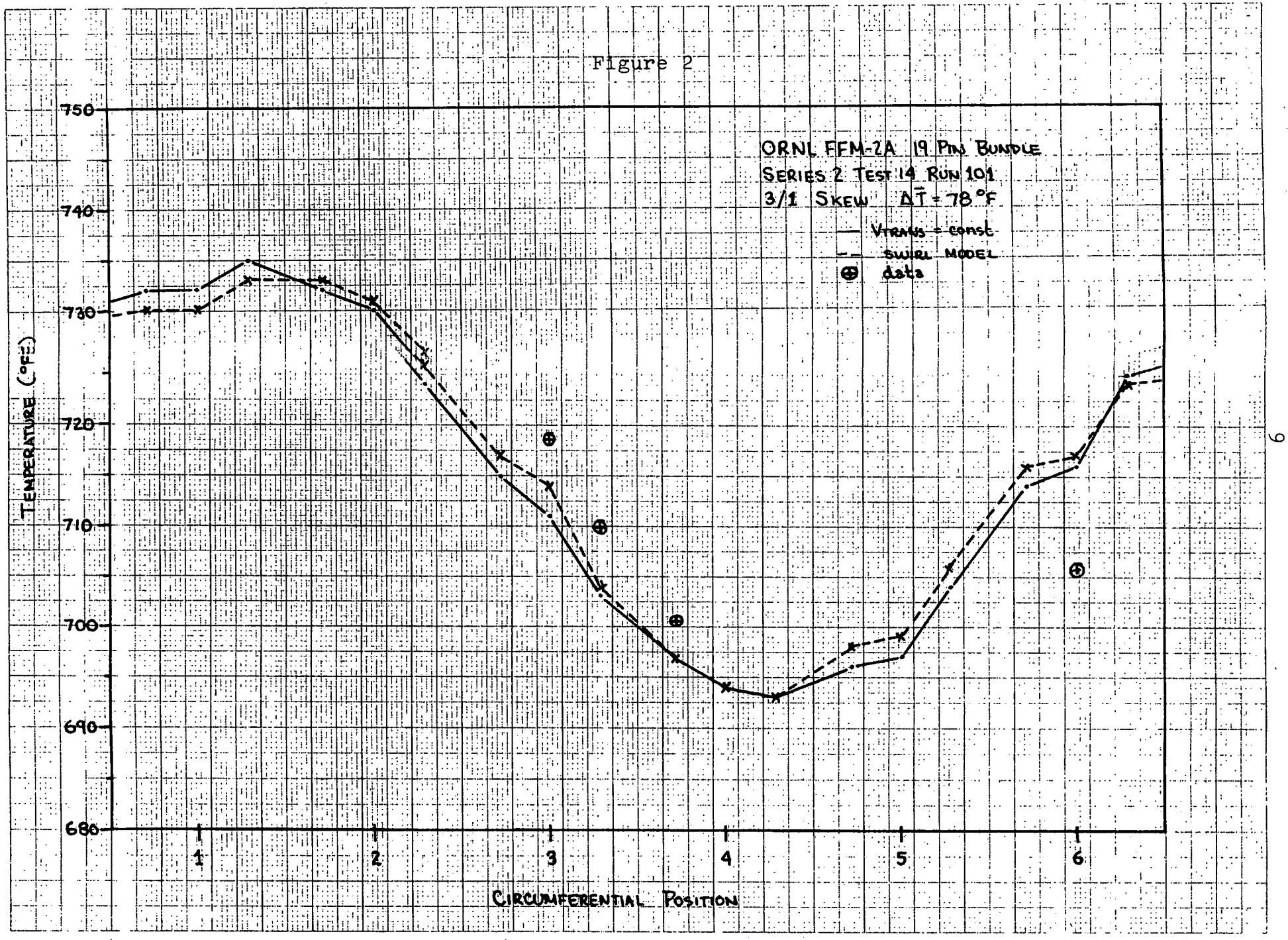

Figure 3

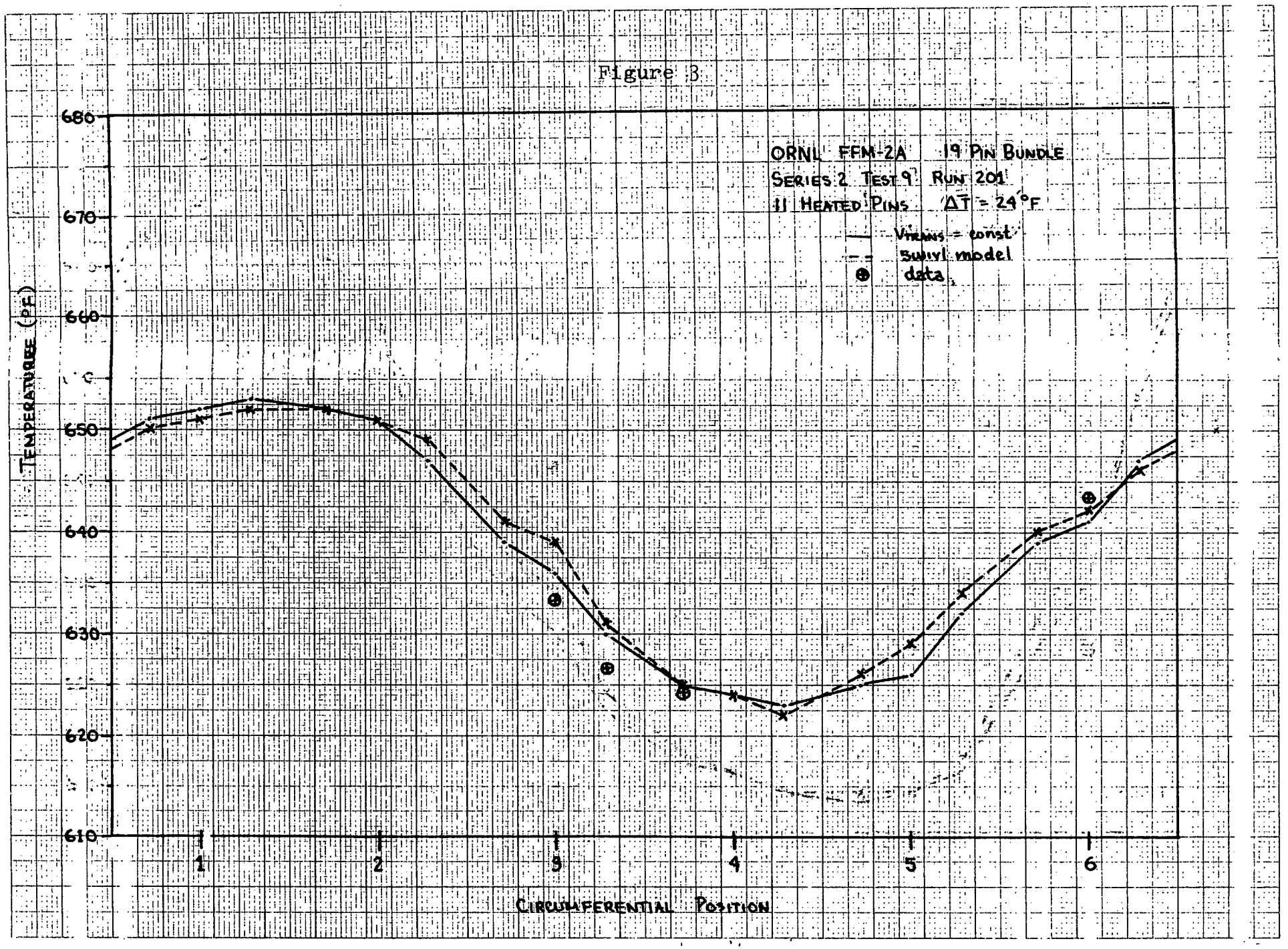

Figure 4

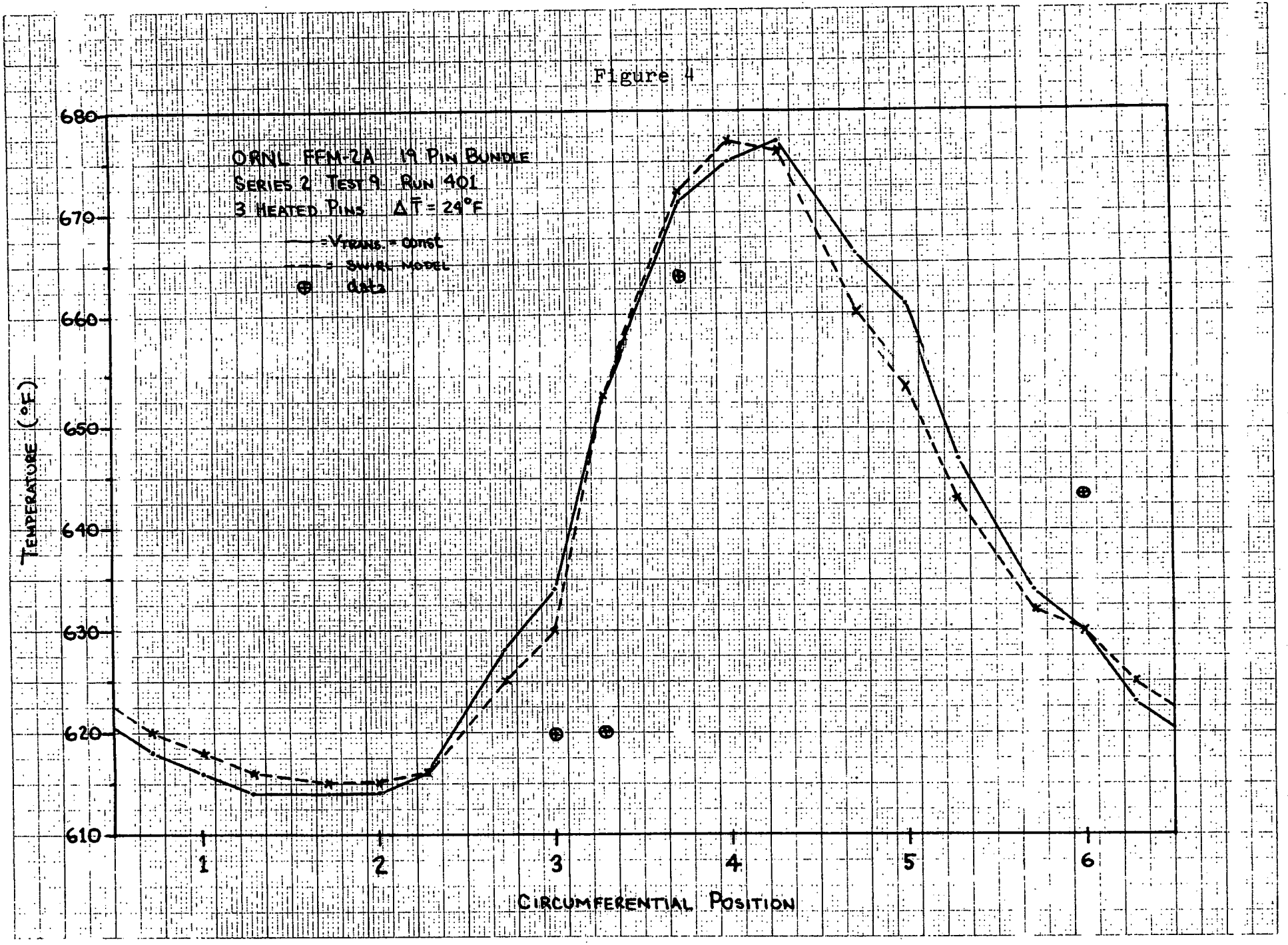

Figure 5

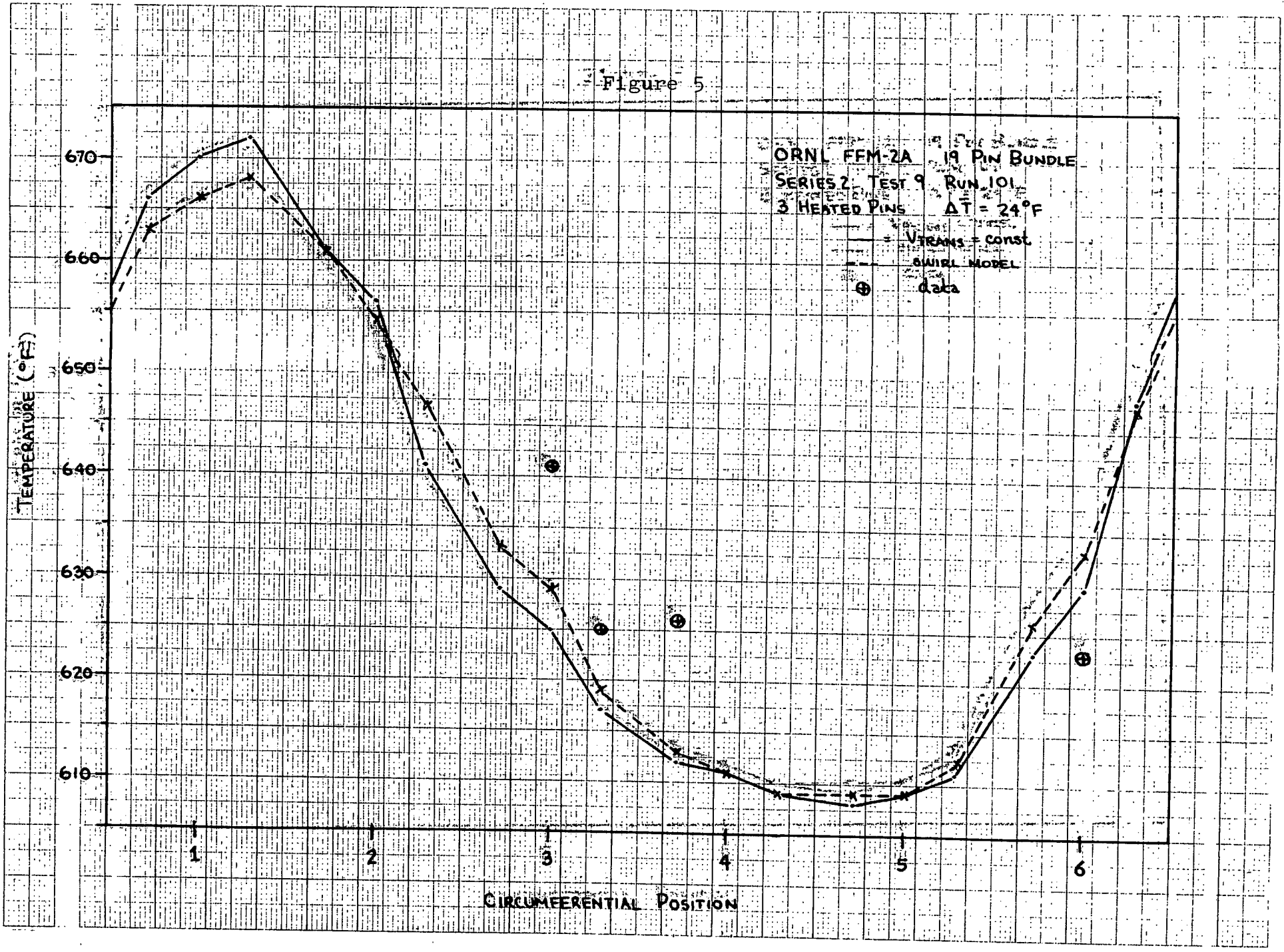

TASK II: SUBCHANNEL GEOMETRY (BARE RODS)

TASK IIA: Assessment of Available Data

Nothing to report this quarter.

TASK IIB: Experimental Subchannel Water Mixing Investigation (Joseph M. Kelly)

This work has been completed for pitch to diameter ratio of 1.10 and will be reported in full in Topical Report COO-2245-42TR.

TASK IIC: Experimental Subchannel Local Parameter Measurements (John Bartzis)

Measurements of mean axial velocity and Reynolds stresses have been performed at C/D = 113 (fully developed flow) and Reynolds numbers 9,000, 26,000 and 66,000. We are in the process of reducing the data.

TASK IIC.1: Wall Shear Stress Measurements (Mohammed Fakory)

The first data measurement was started at the end of January. The schematic diagram of flow circuit is shown in Fig. 1. A compressor supplies air, the supply pressure is within 90-110 psia. A pressure regulator value (PRV) keeps the down stream pressure constant (within a range which is dependent on the flow rate). Gate value (A) can be opened to bleed and remove moisture and dust before running air through the test section. Gate value (B) controls the flow rate. The prechannel section composed of three similar perforated plates (Ref. 1) expands and develops the flow. The last part is a flow meter, details of which are shown in Fig. 2 (Ref. 3). In order to minimize the system pressure drop, a reduced diameter pipe section, 3/8" I.D., was used immediately after the pressure regulator valve.

From initial operation it appeared that either pipe dusts or moisture blocked the tip of the measuring probe. The filter was replaced with the finest available and located as shown close to the prechannel entrance. Also to improve the data reading, a probe of a new design was used. The static pressure in the test section is measured by a 1/16" diameter hole which has been completely deburred (according to Ref. 4).

The difference between the Preston tube pressure and static pressure was measured by the following devices as shown in Fig. 1.

1) Barocel pressure sensor model 570D made by Datametric.

2) Electronic manometer signal conditioner model 1173 made by Datametric for visual monitoring of the pressure difference by means of the pressure sensor DC voltage output.

3) Digital voltmeter to read the signal output with more accuracy.

4) Integrator voltmeter to find the mean value of pressure fluctuation.

The resultant data are shown in Fig. 3. These data were taken with a ten second integrating period. During the experiment two problems appeared. First the source of air was the main laboratory system which had a pressure fluctuation corresponding to the compressor on-off cycle. Specifically the flow rate at maximum line pressure corresponding to the beginning of the compressor off period (110 psig) was different than end of compressor off period (90 psig). This difference in flow rate is very small (less than 0.05" Hg change on the orifice pressure difference monumeter) and could not be suppressed by the pressure regulator value. However because the Barocel pressure sensor is very sensitive, these changes could be seen clearly on the voltmeter. The second problem was fluctuation in ΔP_d reading even when the Preston tube was moved into contact with the wall and was only .008" outside diameter. In order to be sure this fluctuation was not due to compressor period, it was decided to use a blower instead of the laboratory compressed air system. The blower with 1.27" Hg head was installed after the orifice plate flow meter to draw air through the test section. Also to be sure that any effect of peripheral static pressure distribution has been considered, the test section was modified so that the static pressure tap can be rotated over 35°.

One set of measured data after these changes is depicted in Fig. 3 (Curve 1). These data were also taken with a 10 second integrating period because of the pressure fluctuation experience. It appeared that since the pressure fluctuations were still present, they are not

due to compressor period but rather due to the fact that the sublayer region is in fact turbulent. Very accurate and sensitive instruments would be necessary to record the detailed fluctuation if they were of interest. No fluctuation in pressure drop appeared and also at Re number equal to 4568, no peripheral static pressure variation or fluctuation was detected. The Preston tube outside diameter for both of these results was 0.014".

This work will be continued to gather data at higher Re number.

TASK IID: Analytical Model Development - Subchannels (John Bartzis

At this stage we are in the process of fitting the experimental data to determine model constants.

References

(1) Fluid Meters their Theory and Application, Report of ASME Research Committee on Fluid Meters (1971).

(2) Flow Meter Computation Handbook, ASME Research Committee on Fluid Meters (1961).

(3) W.A. Leary and D.H. Tsai, "Metering of Gasses by Means of the ASME Square-Edged Orifice with Flange Tapes," MIT (July 1951).

(4) ASME Power Test Codes (1961).

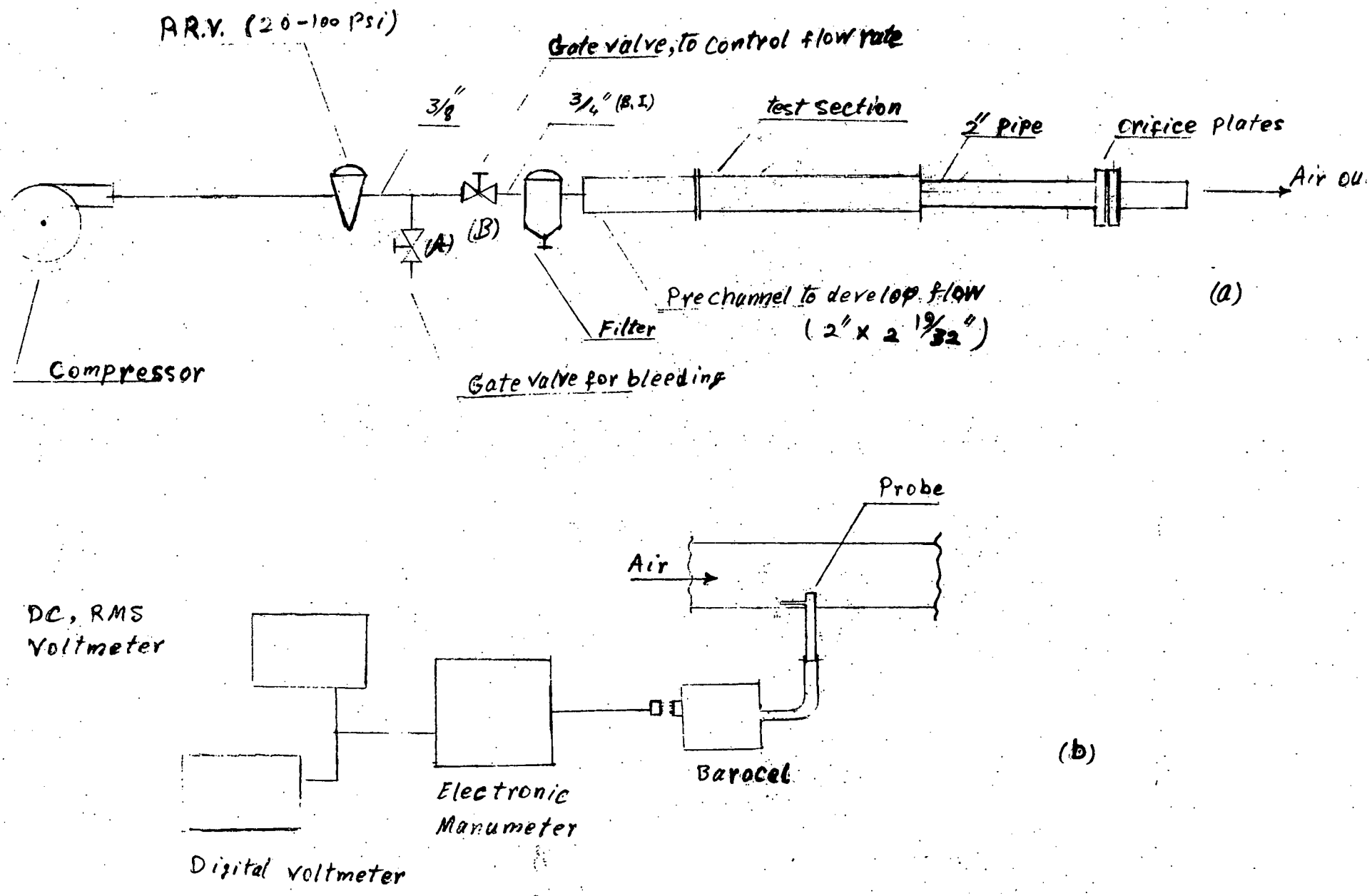
A.R.V. (20-100 Psi)
Gate valve, to control flow rate
3/8"
3/4" (B.I.)
test section
2" pipe
orifice plates
Air ou
(A)
(B)
Prechannel to develop flow
(2" x 2 19/32")
(a)
Filter
Compressor
Gate valve for bleeding
Probe
Air
DC, RMS
Voltmeter
Electronic
Manumeter
Barocel
(b)
Digital voltmeter

Fig. 1

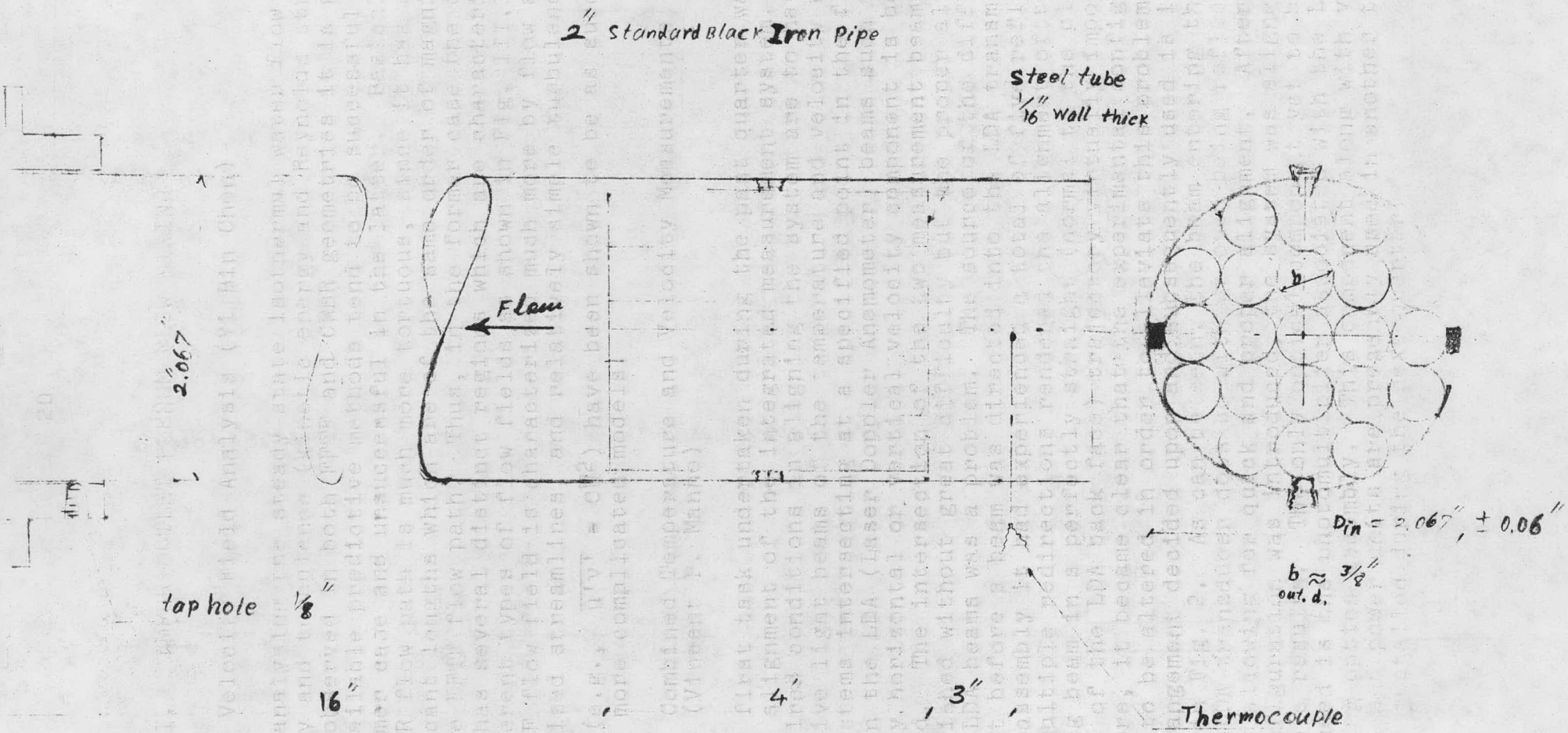
2" Standard Black Iron Pipe
Steel tube
1/16" wall thick
Flow
2.067"
tap hole 1/8"
16"
4"
3"
Thermocouple
b
Din = 2.067", ± 0.06"
b ≈ 3/8"
out. d.

Fig. 2

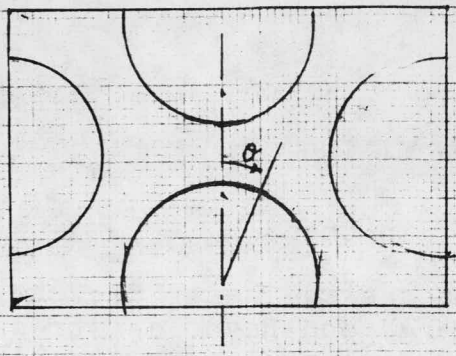

$\frac{\tau_w}{\bar{\tau}_w} = \frac{\tau_w}{\tau_{w_{avg}}}$

1.2
1.1
1.0
0.9
0.8
0.7
0.6
0.5

θ°

Resulted from Curve (1) $\bar{\tau}_w = 3.47 \times 10^{-3}$ lbf/ft²

τ_w lbf/ft²

3×10^{-3}
2×10^{-3}
1×10^{-3}

1.6x
1.5x
1.4x1
1.3x1
1.2x1
1.1x10

(2)

(1) $R_e = \frac{\rho \bar{V} D_h}{\mu} = 4568$

(2) $R_e = \frac{\rho \bar{V} D_h}{\mu} = 9525$ (by using comp.)

By using Patel Correlation

0 2 4 6 8 10 12 14 16 18 20 22 24 26 28 30 32 θ°

TASK III. LMFBR OUTLET PLENUM FLOW MIXING

III.A. Velocity Field Analysis (Yi Bin Chen)

In analyzing the steady state isothermal water flow velocity and turbulence (kinetic energy and Reynolds stress) fields observed in both FFTF and CRBR geometries it is seen that available predictive methods tend to be successful in the former case and unsuccessful in the latter. Basically, the CRBR flow path is much more tortuous, since it has several significant lengths which are of the same order of magnitude, than the FFTF flow path. Thus, in the former case the outlet plenum has several distinct regions which are characterized by different types of flow fields as shown in Fig. III.1a. The FFTF flow field is characterized much more by flow along laminarized streamlines, and relatively simple turbulence models (e.g., $\overline{u'v'} = C\bar{U}^2$) have been shown to be as successful as much more complicated models.

III.B. Combined Temperature and Velocity Measurements (Vincent P. Manno)

The first task undertaken during the past quarter was the optical alignment of the integrated measurement system. The two desired conditions in aligning the system are to have the respective light beams of the temperature and velocity measurement systems intersecting at a specified point in the flow and to align the LDA (Laser Doppler Anemometer) beams such that a purely horizontal or vertical velocity component is being measured. The intersection of the two measurement beams was accomplished without great difficulty but the proper alignment of the LDA beams was a problem. The source of the difficulty was that before a beam was directed into the LDA transmitting optics assembly it had experienced a total of five reflections. These multiple redirections rendered the alignment of the entering beam in a perfectly straight (normal to the plane surface of the LDA back face) trajectory virtually impossible. Therefore, it became clear that the experimental configuration needed to be altered in order to alleviate this problem. The new arrangement decided upon and subsequently used is illustrated in Fig. 2. As can be seen, the beam entering the rear of the LDA transducer does so without ever being reflected; thereby allowing for quick and proper alignment. After this new configuration was introduced, the system was aligned with favorable results. The only optical component yet to be introduced is the photomultiplier associated with the LDA receiving optics assembly. This component along with various control and power units are presently used in another task but will be installed during the next quarter.

As was outlined in the previous progress report, devising the proper flow seeding system has been difficult. The two possible solutions presented in the last report also proved to be unworkable. The creation of a suction in the flow circuit via a reduced area or "Venturi" section failed because the suction produced was not strong enough to entrain a significant amount of seed in the flow. The second alternative of introducing the flow seed via the natural suction of the air blower intake was unsuccessful because the attrition rate of the seeding particles through the heater was much too high. However a new avenue of investigation has been initiated and promises more fruitful results. The new scheme involves the construction and use of a fluidized bed injection system. A fluidized bed is basically a sealed reservoir or canister of particles through which an air flow is passed. If the air flow is great enough, the particles become entrained in the flow in an analogous fashion as vapor bubbles in a fluid. The seeded air flow then exits the fluidized bed and is directed into the flow circuit. The system has two significant positive features -- the seed injection and entrainment are quite uniform and the seed rate can be varied by changing the air flow rate into the canister. The construction of this apparatus has just begun and upon its completion it will be introduced into the experimental configuration.

Whatever seeding system is used, it is clear that the internal faces of the test cell will eventually become occluded due to the deposition of seeding particles. Therefore, periodiccally these clouded faces must be cleaned in order to minimize deleterious scattering of the laser beams. Unfortunately the test cell being used was permanently sealed and proper cleaning of the inside surfaces was impossible. Another undesirable feature of the original test cell was its internal width of 1/4 inch. At velocities present in the cell, questions had arisen as to whether the boundary layer spanned a substantial percentage of the open channel. Therefore, with these limitations in mind, a new test cell was designed and constructed. The internal structure of the new test cell is illustrated in Fig. 2. As can be observed from the initial progress report, the dimensions of the new test cell are nearly identical to the original. There are, however, three significant improvements. In answer to the initial problem outlined above, the new test cell can be taken apart and reassembled easily thereby allowing easy cleaning of the internal faces. The internal width of the new section is 1/2 inch. This reduces the significance of the boundary layer thickness. There is a second effect associated with doubling the internal width of the cell in that the temperature upset the measurement system is sensitive to is reduced by 50%. This effect arises because the product of temperature upset and cell internal thickness must be equal to a constant which is determined by the wavelength of the laser.

Therefore, since the wavelength being utilized has not been altered and the thickness was doubled, the temperature upset is halved. This change, however, does not affect the accuracy of the temperature measurement system. Finally, as can be seen in Fig. 2, the new test cell's internal geometry can be changed as to model both the FFTF and CRBR (Clinch River Breeder Reactor) outlet plenum flow geometry. Also, the new internal geometry has the feature of mixing chimneys which more accurately resembles the actual outlet plenum configurations. This feature of variable FFTF/CRBR geometry will allow us to measure the different turbulent mixing properties of the two designs and further facilitate comparison.

In summary, the work of the next quarter will consist of completing the construction and installment of the fluidized bed into the experiment. Secondly, after the seeding system is in place, the LDA receiving optics and control units will be installed and tested in conjunction with the seeding system. Finally, upon realigning the complete optical system, initial measurements will be undertaken.

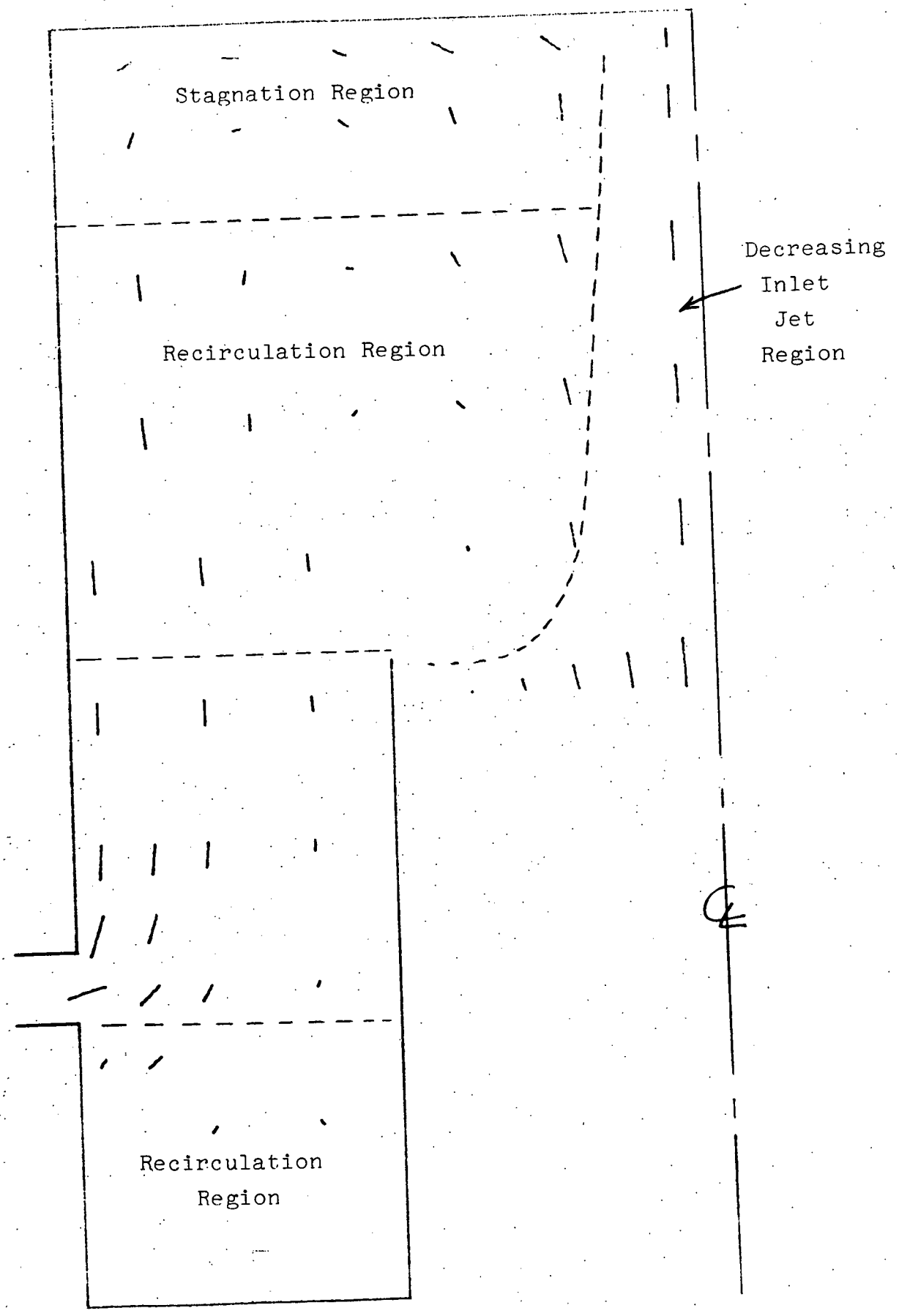

Fig. III.1.a. Qualitative CRBR Flow Field

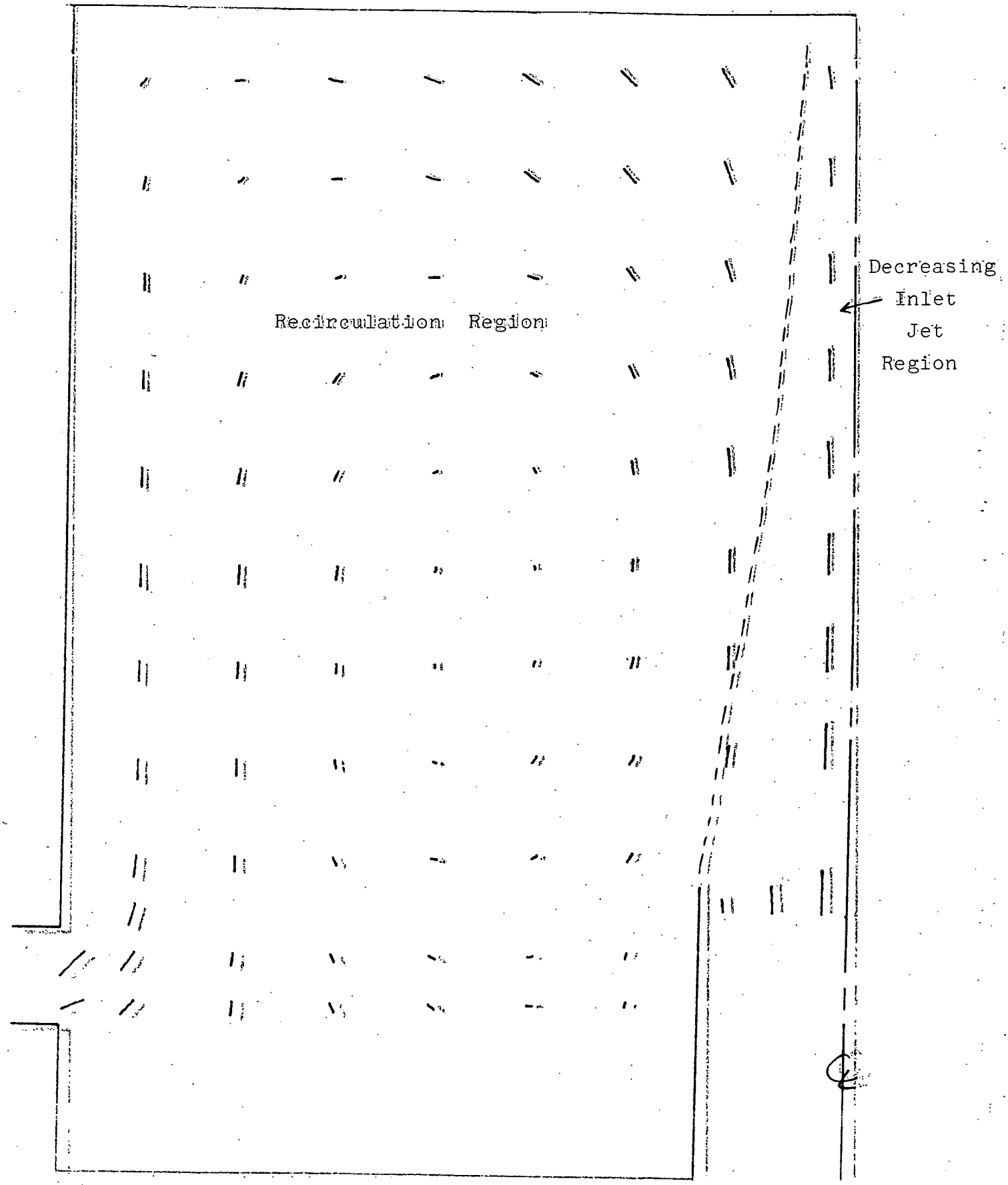

Fig. III.1.b. Qualitative FFTF Flow Field

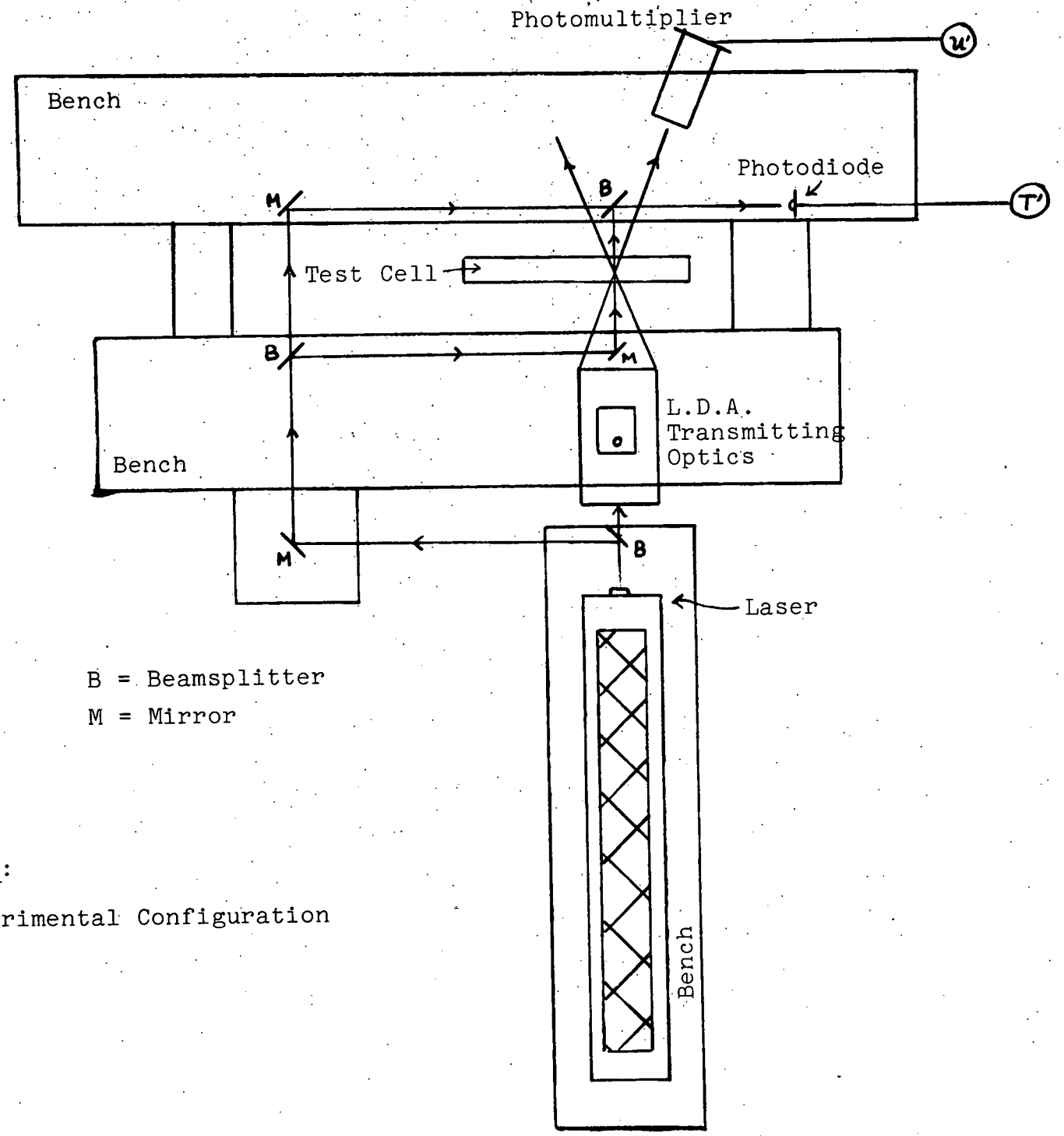

B = Beamsplitter

M = Mirror

Figure III.2:

New Experimental Configuration

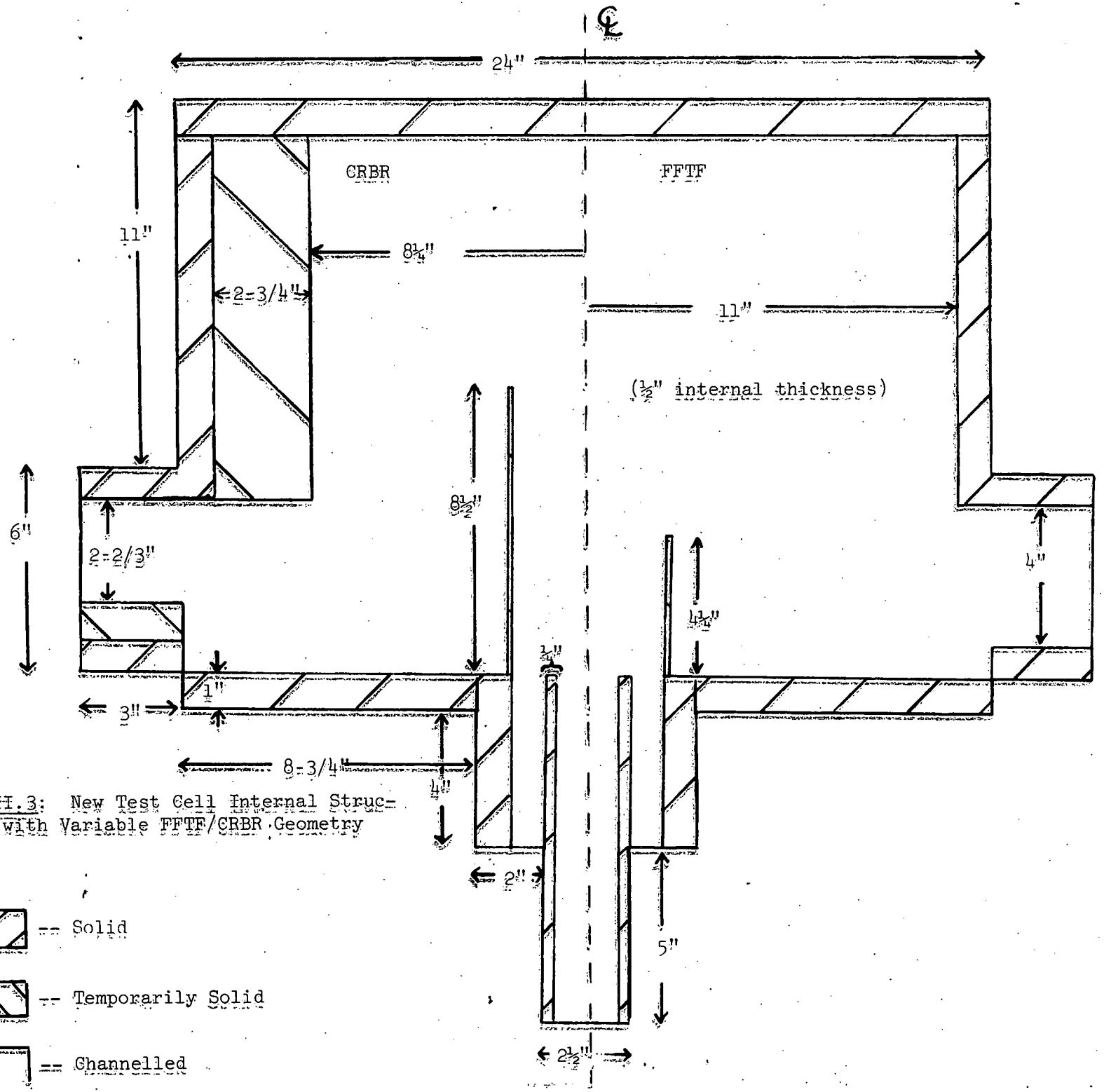

Figure III.3: New Test Cell Internal Structure with Variable FFTF/CRBR Geometry

TASK IV: THEORETICAL DETERMINATION OF LOCAL TEMPERATURE FIELDS IN LMFBR FUEL ROD BUNDLES

TASK IVA: Code Development for Solving the 2-D Multicell Multiregion Energy Equations (Man Kit Yeung)

Summary

During the last quarter, work has been directed to the investigation of the effect of fuel internal disturbances on clad circumferential temperature variations. The internal disturbances are generally caused by off-center pellet location, fuel cracking or non-uniformity of power density in the fuel. All these effects contribute to the circumferential temperature variations on top of the variations induced by the coolant region asymmetries.

It is a well known fact that the power density across a pin is fairly uniform in the core of a LMFBR. However, this does not hold for the radial blanket as strong flux gradient exists throughout the blanket region and a uniform power density approximation will totally fail to represent the true physical problem. This report presents the methodology of modeling the non-uniformity of power generation in the fuel and demonstrates its effect on the circumferential clad temperature variations in various unit cells of a finite LMFBR blanket assembly. Parametric studies showing the effect of the magnitude of the non-uniformity in the power distribution, as well as the changes of the clad thermal conductivity upon the circumferential clad temperature variations are also given in the present report.

1. Governing Differential Equations and Modeling of the Power Non-Uniformity

Consider an arbitrary polygonal unit cell as shown in Fig. 1. The region consists of the nuclear fuel for $0 \leq r \leq a$ and $0 \leq \phi \leq \pi$. The clad for $a \leq r \leq b$ and $0 \leq \phi \leq \pi$, and the coolant for $b \leq r \leq a_1/\cos(\phi - d_1)$. The domain of ϕ ranges from 0 to π which is the symmetry section of the unit cell being considered.

By neglecting axial conduction effect, the temperature fields in the fuel (v) and the clad region (t) respectively, satisfy Poisson's equation:

$$\frac{1}{r}\frac{\partial}{\partial r}\left(r\frac{\partial v}{\partial r}\right) + \frac{1}{r^2}\frac{\partial^2 v}{\partial \phi^2} + \frac{q'''}{k_f} = 0 \qquad (1)$$

and Laplace equation:

$$\frac{1}{r}\frac{\partial}{\partial r}\left(r\frac{\partial t}{\partial r}\right) + \frac{1}{r^2}\frac{\partial^2 t}{\partial \phi^2} = 0 \qquad (2)$$

respectively, where q''' is the power density and k_f is the thermal conductivity of the fuel.

For the two-dimensional heat source distribution the following expression can be used [1]:

$$q'''(r\phi) = q_B'''(P_i + \delta_i r\cos\phi)\, e^{\zeta_i r^2} \qquad (3)$$

where

P_i = radial peaking factor of row i

q_B''' = average heat source density of bundle

δ_i = tilting parameter of row i

ζ_i = self-shielding parameter of row i

Thus Eq. (3) is flexible enough to take both flux tilting and self-shielding effects into account. Naturally, the empirical tilting and self-shielding parameters have to be fitted either to experimental measurements or neutron calculational results.

Fig. 2 qualitatively shows the different kinds of power densities which can be simulated by setting one or two of the aforementioned parameters equal to zero. It is generally true that the self-shielding effect in a LMFBR is relatively small compared to that of a LWR. Therefore, the clad circumferential temperature variation due to strong neutron flux gradient becomes of prime importance. For a single cell analysis Eq. (3) reduces under these circumstances to:

$$q'''(r\cdot\phi) = q_o'''(1 + \delta r\cos\phi) \qquad (4)$$

On the other hand, with the viscous terms and the axial conduction effect neglected, the energy equation for the coolant region can be written as:

$$\frac{1}{r}\frac{\partial}{\partial r}\left(r\frac{\partial T}{\partial r}\right) + \frac{1}{r^2}\frac{\partial^2 T}{\partial \phi^2} = \frac{\rho c_p u}{k_c}\left(\frac{\partial T}{\partial z}\right) \qquad (5)$$

where

c_p = specific heat of the coolant

k_c = thermal conductivity of the coolant

u = coolant flow velocity

$\left(\frac{\partial T}{\partial z}\right)$ = axial temperature gradient

Two assumptions have been made in order to simplify the analysis. First, slug flow is used to approximate the turbulent flow, i.e., u = constant. Secondly, the flow is assumed to be thermally fully developed. Therefore, the axial temperature gradient is constant and can be determined from the energy balance as

$$\left(\frac{\partial T}{\partial z}\right) = \frac{\pi a^2 q_o'''}{2\rho u A_f c_p} \tag{6}$$

where A_f is the cross-sectional area of the coolant region.

In addition to the governing differential equations, the following boundary conditions have to be satisfied by the temperature fields of fuel, clad and coolant:

$$\frac{\partial v}{\partial \phi}(r,0) = \frac{\partial v}{\partial \phi}(r,\pi) = 0 \tag{7}$$

$$\frac{\partial t}{\partial \phi}(r,0) = \frac{\partial t}{\partial \phi}(r,\pi) = 0 \tag{8}$$

$$\frac{\partial T}{\partial \phi}(r,0) = \frac{\partial T}{\partial \phi}(r,\pi) = 0 \tag{9}$$

$$-k_f \frac{\partial v}{\partial r}(a,\phi) = h_s\{v(a,\phi) - t(a,\phi)\} \tag{10}$$

$$-k \frac{\partial t}{\partial r}(b,\phi) = h\{t(b,\phi) - T(b,\phi)\} \tag{11}$$

$$k_f \frac{\partial v}{\partial r}(a,\phi) = k \frac{\partial t}{\partial v}(a,\phi) \tag{12}$$

$$k \frac{\partial t}{\partial r}(b,\phi) = k_c \frac{\partial T}{\partial r}(b,\phi) \tag{13}$$

Substituting Eqs. (4) and (6) into Eqs. (1) and (5) respectively, Eqs. (1), (2) and (5) can be solved simultaneously by coupling the solutions of the temperature fields with the appropriate boundary conditions. The dimensionless temperature field in the fuel region can be represented as:

$$\frac{v(r,\phi) - A_o}{q_o''' a^2/2k_c} = \frac{1}{2}\left[1 - \left(\frac{\rho}{t}\right)^2\right]\left(1 + \frac{\delta b}{2}\rho\cos\phi\right) + \sum_{n=1}^{\infty} \frac{Y_n}{n}\rho^n \cos n\phi \tag{14}$$

whereas the temperature field in the clad is given by:

$$\frac{t(r,\phi) - A_o}{q'''_o a^2/2k_c} = \frac{1}{\kappa} \ln \frac{t}{\rho} - \frac{1}{Bi_s} \frac{1}{\kappa\kappa_w}$$

$$- \frac{3\delta b \cos\phi}{16\kappa\kappa_w} \{\rho(\frac{1}{Bi_s} + \frac{1}{3} + \kappa_w)$$

$$+ t^2(\frac{1}{Bi_s} + \frac{1}{3} - \kappa_w)\rho^{-1}\}$$

$$+ \sum_{n=1}^{\infty} \frac{Y_n}{2n} \{\rho^n(1 + \kappa_w + \frac{n}{Bi_s})$$

$$+ t^{2n}\rho^{-n}(1 - \kappa_w + \frac{n}{Bi_s})\}\cos n\phi \qquad (15)$$

The temperature field in the coolant region can be calculated from:

$$\frac{T(r,\phi) - A_o}{q'''_o a^2/2k_c} = \frac{1}{\kappa}(\ln t - \frac{1}{Bi}) - \frac{1}{\kappa\kappa_w}(\frac{1}{Bi_s}) - (1 + \frac{1}{1})\ln\rho$$

$$+ \frac{1}{2}(\rho^2 - 1) - \frac{3\delta b \cos\phi}{16\kappa\kappa_w}(t_1\rho - s_1\rho^{-1})$$

$$+ \sum_{n=1}^{\infty} \frac{Y_n}{n} [f_n\rho^{-n} + g_n\rho^n] \cos n\phi \qquad (16)$$

where

$$t_1 = (\frac{1}{Bi_s} + \frac{1}{3} + \kappa_w)(\frac{1}{Bi} + 1 + \kappa) + (\frac{a}{b})^2(\frac{1}{Bi_s} + \frac{1}{3} - \kappa_w)$$

$$(1 - \frac{1}{Bi} - \kappa);$$

$$s_1 = (\frac{1}{Bi_s} + \frac{1}{3} + \kappa_w)(\frac{1}{Bi} + 1 - \kappa) + (\frac{a}{b})^2(\frac{1}{Bi_s} + \frac{1}{3} - \kappa_w)$$

$$(1 - \frac{1}{Bi} + \kappa);$$

$$f_n = \frac{1}{4}\left[\left(1 + \kappa_w + \frac{n}{Bi_s}\right)\left(1 - \kappa + \frac{n}{Bi}\right) + \left(\frac{a}{b}\right)^{2n}\left(1 - \kappa_w + \frac{n}{Bi_s}\right)\left(1 + \kappa - \frac{n}{Bi}\right)\right],$$

$$g_n = \frac{1}{4}\left[\left(1 + \kappa_w + \frac{n}{Bi_s}\right)\left(1 + \kappa + \frac{n}{Bi}\right) + \left(\frac{a}{b}\right)^{2n}\left(1 - \kappa_w + \frac{n}{Bi_s}\right)\left(1 - \kappa - \frac{n}{Bi}\right)\right],$$

$$\kappa_w = \frac{k_f}{k}, \qquad \kappa = \frac{k}{k_c}, \qquad Bi_s = \frac{h_s a}{k_f}, \qquad Bi = \frac{hb}{k},$$

$$\rho = \frac{r}{b}, \qquad \text{and} \qquad I = \frac{2A_f}{\pi a^2}.$$

Naturally the Fourier series shown in Eqs. (14), (15), and (16) have to be approximated by truncating at a finite number of terms. Once the Fourier coefficients Y_n have been determined by solving the set of linear equations resulting from a boundary least square procedure [2] the temperature fields in the three regions are immediately obtained. Formal derivations of the procedure will be given elsewhere and only the calculational results are presented in what follows.

2. Results

2.1 Effect of Different Power Tilting Parameters

The thermal and geometric parameters used for the calculations given in Table 1 are typical design values for current LMFBR blanket assemblies [3]. The dimensionless power tilting parameter, δb, is varied from -0.10 to 0.10, which represents roughly about 22% power tilting across the fuel region of the rod. It is illustrated by Fig. 3 that the introduction of a negative power tilting parameter for a corner cell results in an increase of the clad circumferential temperature variation. This is because the effect of power tilting has been added on top of the geometric irregularity of the coolant region, i.e. the power is increased in the region where the coolant is already hot and decreased where the coolant is already greatly undercooled. This kind of unfavorable combination of power tilting and geometry leads to an increase of approximately 0.7 in the dimensionless clad temperature variation, which, for typical operating conditions, means 30° to 60°F depending on the location of the rod in the blanket. On the other hand, for cases with positive tilting parameters, the circumferential clad temperature variations decrease because the

geometric irregularity and the power non-uniformity have been favorably combined such that they offset each other. The same argument holds for the clad temperature distributions of the side cell as shown in Fig. 4. However, this is not the case for the internal cell because it already has a very high degree of geometric symmetry, which results in a fairly small clad temperature variation. Therefore, any power tilting in either direction will immediately lead to a breakdown of the temperature symmetry and results in an increase of the clad circumferential temperature variation as shown in Fig. 5.

It should be noticed that although this analysis considers the power tilting only along the $0,\pi$ direction, the maximum temperature variations for tilts along other directions should be bounded by the results of the former. Naturally, the local behavior of the temperature field changes from case to case.

Figs. 6a and 6b summarize the sensitivity of the power tilting effect on the clad temperature variations by plotting the normalized maximum clad temperature difference ΔT_{max}^*, defined as:

$$\Delta T_{max}^* = \frac{(T_{\text{hot spot}} - T_{\text{cold spot}})_{\delta b}}{(T_{\text{hot spot}} - T_{\text{cold spot}})_{\delta b=0}} \qquad (17)$$

vs. the dimensionless tilting parameter δb. These curves provide an indication for the sensitivity of the clad temperature variation of a unit cell to the power tilting effect, as well as a correction for clad azimuthal temperature variation used in structural analyses.

It is seen from the two figures that the relationships between ΔT_{max}^* and δb for the three characteristic unit cells are basically linear over the range of interest. Furthermore, the corner and side cells are almost equally sensitive to the power tilting in the fuel region; i.e., a change of approximately 22% in ΔT_{max}^* results from a 22% power tilt across the rod. On the other hand, the same power tilting in the internal cell induces a 600% increase in clad temperature variation. However, at this point, it should be recalled that the clad temperature variation in an internal cell has a constant power profile across the fuel ranges only from 4-10°C.

2.2 Effect of Clad Thermal Conductivity

Three calculations with different clad conductivities and a tilting parameter of -0.10 are performed for the corner and the 4-side internal cell. As shown in Table 2, the thermal conductivities of coolant and fuel have been kept constant in order to illustrate the effect of the clad thermal conductivity. Both Figs. 7 and 8 demonstrate, as expected, that the circumferential clad outside temperature variation decreases as the

clad thermal conductivity increases. This is due to the fact that the higher clad thermal conductivity enhances azimuthal heat conduction in the clad region and thus reduces the angular temperature gradient which results from the strong power tilting in the fuel region. However, it is also observed that the clad temperature variation is relatively insensitive to clad thermal conductivity variations. For instance, a four-time increase in clad thermal conductivity for a corner cell results in a decrease of 0.55 in dimensionless maximum temperature variation which is approximately equal to 20-40°F for blanket pins under normal operating conditions.

2.3 Conclusions and Discussion

The aforementioned results have led to the following conclusions:

1) Under normal operating conditions, the clad temperature variations of the unit cells on the periphery of the bundle are primarily governed by the geometric irregularity of the coolant region. Internal disturbance due to power tilting has relatively small effect on the azimuthal clad temperature variations.

2) The internal cell itself is in a highly symmetric configuration which contributes little to the circumferential clad temperature variation. Therefore, power non-uniformity in the fuel region due to neutron flux gradient is the controlling mechanism for the clad temperature variation.

3) Due to the physical limitation of the clad dimension for the blanket rods (a/b = 0.94), substantial reduction in circumferential clad temperature variation cannot be achieved simply by changing the clad thermal conductivity.

TASK IV.B: 3-D COUPLED TWO CELL SLUG FLOW HEAT TRANSFER ANALYSIS (Chung Nin Wong)

Summary

During the last quarter, work has been focused on solving the temperature profile of the coupled cell problem with a non-uniform axial power distribution in both fuel pins. Furthermore, the calculation of the effective conduction mixing length as a function of the axial distance has been initiated and first preliminary results are presented.

1. 3-D, Two-Cell Analysis with Non-uniform Axial Power Distribution

In deriving the previously presented results [4], the assumption of an axially uniform heat flux distribution has been made. In reality, the axial flux profiles may be fairly well represented by sinusoidal shapes. In order to account for this additional effect, Duhamel's Superposition Principle in the following form is used:

$$\theta(\delta,\phi,\xi) = \theta_c(\delta,\phi,\xi)q''(0) + \int_0^{\xi}\theta_c(\delta,\phi,\xi-\psi)\frac{dq''(\psi)}{d\psi}\,d\psi \qquad (1)$$

where

$\theta_c(\delta,\phi,\xi)$ = temperature field obtained by assuming $q''\neq f(\xi)$

$q''(0)$ = heat flux at $\xi = 0$

ξ = dummy independent variable

By virtue of this theorem, it is possible to generate the temperature profile for the axially non-uniform flux profile once the temperature field for the uniform axial heat flux profile has been obtained. The results for the latter have been reported in [4].

2. Results

The fuel assembly of the CRBRP has been chosen as the base case for showing the effect of a non-uniform axial heat flux shape upon the temperature fields. The design values taken from the PSAR are summarized below:

P/D = 1.24

2W/D = 1.42

D = 0.23 in

H = 3 ft

T_{in} = 730°F

Pe = 357

F_q = 1.24

$\bar{q}'$ = 6.67 kw/ft

$q''(z) = q_o'' \sin\left(\frac{\pi(z + H_e/2 - H/2)}{H_e}\right)$

H_e = 4.59 ft

q_o'' = 3.78×10^5 Btu/ft^{2}hr

Fig. 9 shows the outside clad temperature of the corner pin for various axial locations for both the single-cell and two-cell analysis. The coupled analysis leads to a slight increase in the azimuthal temperature variation around the fuel pin. This increase, however, is not as large as that shown in Fig. 8 of [4] for P/D = 1.3. On the other hand, Fig. 9 shows again the typical "bump" in the clad temperature distribution for the coupled analysis for the axially non-uniform flux profile, too, which has been already observed for the uniform heat flux case in [4].

Fig. 10 compares the temperature profiles of a two-cell analysis with uniform and non-uniform heat flux shapes. For the parameters chosen, the uniform axial flux shape results in a somewhat higher average temperature of the clad which consequently leads also to higher maximum clad temperatures at ϕ = 180 degrees.

3. Effective Conduction Mixing Length in Three Dimensions

Values for the effective conduction mixing length have already been reported in [4] for the 2-D thermally fully-developed multiregion analysis. These results were implemented into COBRA-IIIC and it has been shown [5] that the use of correctly derived L_{ij} instead of setting L_{ij} = 1 results in a decrease of subchannel temperature gradients. However, it is fully understood that using L_{ij}'s derived from thermally fully-developed conditions gives only preliminary and approximate results, too, although these results show at least the correct effect of the geometry as compared to the common approach of setting L_{ij} = 1. What is missing, though, is the thermal. entrance effect, which has a major impact upon the temperature field as shown in the preceding progress reports.

The heat transfer rate due to conduction across the common boundary between adjacent subchannels i and j as shown in

Fig. 11 is given by

$$Q_{ij} = k \frac{S_{ij}(\overline{T_i} - \overline{T_j})}{\ell_{ij}} \tag{1}$$

which can be reformulated as

$$Q_{ij} = k \frac{S_{ij}}{\ell_{ij}^*} (\overline{T_i} - \overline{T_j}) \frac{1}{L_{ij}} \tag{2}$$

where

S_{ij} = length of the common boundary

ℓ_{ij}^* = centroid-to-centroid distance

ℓ_{ij} = effective conduction mixing length

$L_{ij} = \frac{\ell_{ij}}{\ell_{ij}^*}$

In a first approach, ℓ_{ij} has been made dimensionless by using the pitch, P, rather than using the centroid-to-centroid distance, ℓ_{ij}^*. This leads to

$$\ell_{ij}^+ = \frac{\ell_{ij}}{P/2} \tag{3}$$

and furthermore to

$$\ell_{ij}^+ = k \frac{\overline{\theta}_i - \overline{\theta}_j}{\frac{1}{S_{ij}} \phi_{ij}} \tag{4}$$

where

$$\overline{\theta}_{i,j} = \frac{\overline{T}_{i,j} - \overline{T}_{in}}{q_o'' r_f / k} \tag{5}$$

$$s_{ij} = \frac{S_{ij}}{P/2} \tag{6}$$

$$\phi_{ij} = \frac{Q_{ij}}{\frac{q_o'' r_f}{k} \frac{1}{P/2}} \tag{7}$$

Obtaining the average subchannel coolant temperatures efficiently poses a problem for the entrance part of the overall solution. For this purpose a special subroutine has been developed.

4. Preliminary Results for the Effective Conduction Mixing Length

The geometric and thermal parameters of the Karlsruhe experiment [6] were chosen to obtain preliminary results. For convenience these parameters are again summarized below:

$P/D = 1.3$

$2W/D = 1.38$

$P_e = 372$

$D = 9$ mm

$T_{in} = 415°C$

$\bar{q}'' = 104$ W/cm^2

$q''(z) =$ constant

The results for ϕ_{ji} and ℓ_{ij}^+ as functions of the axial coordinate are given below:

z [mm]	ϕ_{ji}	ℓ_{ij}^+
115	0.2705	2.7696
295	0.4141	1.8803
475	0.5156	1.5608
655	0.5932	1.396
1000	0.7003	1.2372
1500	0.8011	1.1347
th. fully-developed	1.0367	0.9868

It should be understood that the results shown in the table are still of preliminary nature inasmuch as no sensitivity study has been made yet to determine how the number of harmonics and eigenvalues kept in the solution may affect the ℓ_{ij}^+. However, it is felt that a best estimate solution is not needed at this point in time. Future work will concentrate upon the impact of the accuracy in ℓ_{ij}^+ on the final COBRA-IIIC results.

The table reveals that the heat transfer rate from the internal to the corner subchannel steadily increases from the inlet towards the exit of the core, whereas ℓ_{ij}^+ continuously decreases. It is obvious from these first results that the thermal entrance effect has indeed a major impact upon the mixing.

5. Future Work

Future work will concentrate upon including non-uniform axial heat flux shapes into the analysis. Furthermore, different values for the average heat flux will be considered for the internal and corner pins in order to simulate a flux tilt across the bundle.

Work will continue to modify COBRA-IIIC such that the code can accept axially varying effective conduction mixing lengths in the future. This information will be supplied to the code as a fitted curve and comparisons will be made with the current subchannel approach as well as the modified version using mixing lengths stemming from analyses using the assumption of thermally fully-developed heat transfer.

After enough insight has been gained about the local and global thermal behavior of the bundle wall near region additional efforts will be made to obtain the thermal characteristics of the subchannels constituting the bundle center region. When this information becomes available, COBRA-IIIC will have been made flexible enough to accept regionwise different effective conduction mixing lengths which vary axially.

TASK IV.C: FULLY DEVELOPED LAMINAR MIXED CONVECTION
(Jong-Yue Kim)

Summary

Basically, work has been completed on this subproject, although in the meantime some additional features have been added to the code such as the determination of the reference temperature of the outside clad surface at $\theta = 0$ degrees. This enables the code to calculate non-dimensionless temperature fields for different Ra-numbers. Additional calculations were made for a typical CRBR blanket assembly for a set of typical Ra-numbers. These results then were used as input to a 2-D thermoelastic and 1-D inelastic clad analysis as described in Task IV.D.

TASK IV.D: 2-D THERMOELASTIC AND INELASTIC CLAD ANALYSIS (R. Karimi)

Summary

After having achieved appreciable progress in the subtasks IV.A and IV.B and finished subtask IV.C, it has been decided to couple directly the local thermal analysis to a structural thermoelastic and inelastic code because a literature study revealed that no coupled computer code for this purpose exists yet.

During the last quarter, work has been completed for the 2-D thermoelastic analysis. In addition, the inelastic study using a 1-D code has been finished. The results of both analyses are summarized in [7].

In the meantime, work has been initiated to integrate the thermal single-cell, multiregion analysis into a 2-D inelastic analysis code in order to obtain values for local damage of the clad.

The final goal of this combined thermal-structural study is to obtain displacements from the structural part of the code in order to feed these back into the thermal part to study their effects upon the thermal analysis. As a result, new displacements will be calculated and so forth. Finally, an iterative procedure will be developed.

1. 2-D Thermoelastic Analysis

The thermoelastic analyses were performed by using the analytical methods described in [8] and [9]. The former analysis incorporates the possibility of accounting simultaneously for either pellet eccentricity or cladding ovality together with a superimposed power tilt across the fuel. In addition, this code accepts circumferentially varying heat transfer coefficients. During the course of this work, the capabilities of the code have been enlarged by incorporating the determination of bending moments and the thermal bowing of the clad. No mechanical grid spacer interactions are considered yet, however. The SEGPIPE code [9] on the other hand accepts only pointwise temperature values at the inside and outside clad surfaces. For this study, these temperatures are obtained from the 2-D single-cell multiregion analysis and are fed as input into the code.

2. Inelastic Analysis

Although the thermoelastic analysis provides some insight into the structural problems, its application is limited to the analysis of clads during the very early stage of burnup. Thus,

in order to cope with more realistic conditions at higher burnups, a computational tool is needed which accounts for creep and swelling effects. In order to gain first insights into these kinds of problems, it was decided to use a one-dimensional representation in the first place. A literature search revealed that the GRO II-code developed by GE [10] fit out purpose best, because it was inexpensive to run and yet gave reasonably correct though approximate solutions.

In order to check the validity of the approach used in GRO-II, the two-dimensional nonlinear structural analysis code GOGO [11] has been made operational in the meantime. The code models all nonlinear effects which are relevant to LMFBR clad operational conditions with the exception of a realistic fuel-clad interaction mechanism. The code as developed and obviously used by GE contains a very crude description of the two-dimensional clad temperature field. Thus, emphasis has been put into the development and integration of a module calculating more realistic temperature fields by using the concepts described in the preceding progress reports.

3. Results

In a first step typical CRBRP fuel and blanket pins have been studied. The results of the thermoelastic analysis are given in detail in [7]. In summary, it was found that the blanket clad experiences about twice the radial displacement of the fuel rod. A parametric study with respect to the effect of the wall distance revealed that the circumferential variation of the radial displacement is largest for large wall distances. In case of a power tilt across the blanket bundle, the circumferential variation of the displacement is largest if the tilt is directed towards the assembly wall. Overall, these first results indicate that the corner rod moves towards the interior rod and hence reduces the coolant cross-sectional area in a regime which is already characterized by high temperatures. Thus, the feedback effects will lead to even higher clad temperatures.

Figs. 12 and 13 summarize the results of the preliminary study for the total creep in blanket and fuel pin clads using GRO-II. Due to the simplified 1-D representation in this code it is assumed that the claddings are either characterized by an average temperature which is typically obtained, say by subchannel codes or by the maximum midwall temperature found by the accurate 2-D thermal analysis. As Fig. 12 depicts, the total creep is about an order of magnitude higher for the latter option. It should be noticed that the circumferential variation of the cladding creep is approximately bounded by the two lines given in this figure. The variation obviously increases with burnup.

For the fuel pin clad Fig. 13 shows a similar behavior over most of its burnup in case of 20% CW 316 SS as cladding material. However, about halfway through the lifetime of the fuel assembly the circumferential creep variation decreases and from 8% burnup on the fuel rod clad nearly creeps uniformly. Annealed 316 SS as clad material behaves quite differently. There the cooler parts creep more than the hotter ones and this difference increases with burnup. From an overall design point of view this may be a desirable feature because it would mean that the cross-sectional area of undercooled coolant is reduced, hence equalizing the temperature variation overall. Naturally, these findings largely rely upon the correlations used for the material properties used by GRO-II.

4. Future Work

Future work will concentrate upon the 2-D inelastic analysis. Emphasis will be put towards the development of an integrated computational tool. Once experience with the resultant code has been obtained in two dimensions, the structural module will be attached to the 3-D two-cell thermal analysis developed in Task IV.B in order to determine the inelastic 2-D displacements at different axial locations. This should give the realistic results for thermal bowing effects and the resulting feedback from bundle wall displacements due to interassembly mechanical interactions.

REFERENCES

1. Boeuf, A., Tassan, S., "A Measurement of the Fine Structure Distribution of the Thermal Flux in Organic Cooled Elements in a D_2O Moderated Lattice," Energia Nucleare 11 (1964, 533).

2. Ng, S.F., "A Collocation Least Square Solution of Boundary Value Problems in Applied Mechanics," Proceedings of the University of Waterloo, Nov. 13, 1971. G.M. Gladwell, Editor.

3. Tagishi, A. and Driscoll, M.J., "The Effect of Reactor Size on the Breeding Economics of LMFBR Blankets," COO-2250-13, MITNE-168, Dept. of Nucl. Engr., MIT, Feb. 1975.

4. Coolant Mixing in LMFBR Rod Bundles and Outlet Plenum Mixing Transients, Progress Report: September 1, 1976-November 30, 1976, Department of Nuclear Engineering, MIT, COO-2245-34.

5. Yeung, M.K., Wolf, L., "Effective Conduction Mixing Lengths for Subchannel Analysis of Finite Hexagonal LMFBR Bundles," ANS Meeting, New York, June 1977.

6. Möller, R. et al., "Experimental Determination of Temperature Fields in Sodium-Cooled, Hexagonal Bundles with Grid Spacers," KFK-2356, 1977

7. Wolf, L., Karimi, R. et al., "2-D Thermoelastic Analysis of LMFBR Fuel Rod Claddings," 4th Int. Conf. Structural Mechanics in Reactor Technology, San Francisco, Aug. 1977, paper C4/d.

8. Wolf, L., "Thermo-Elastic Stresses in Fuel Element Clads Due to the Combined Effects of Flux Tilt in the Fuel and Circumferential Variations of Boundary Conditions," Proc. 2nd Int. Conf. SMIRT, Berlin, Germany, Sept. 10-14, 1973, paper C3/4.

9. Grozier, R.J.M.,"'SEGPIPE': A Program to Determine Thermo-Elastic Deformations in a Segment of a Hollow Cylinder," AECL-4056, 1971.

10. Patel, M., White, D.E., "GRO-II: A Simplified Method for Predicting Mixed Oxide Fuel Rod Performance During Normal Operation," GEAP-14051, 1975.

11. Sim, R.G., "GOGO User's Manual," GEAP-13968, 1973.

Table 1

Geometric and Thermal Parameters Used in the Analysis

$P/D = 1.077$

$2w/D = 1096$

$a/b = 0.94$

$\kappa = \frac{k}{kc} = 0.4$

$\kappa_w = k_f/k = 0.133$

$Bi_s = h_s a/k_f = 10$

$Bi = hb/k = 10^6$

Table 2

Thermal Conductivities Used for Parametric Study

Case	Coolant Thermal Conductivity k_c (BTU/ft-hr°F)	Clad Thermal Conductivity k (BTU/ft-hr°F)	Fuel Thermal Conductivity k_f (BTU/ft-hr°F)	$\kappa = \frac{k}{k_c}$	$\kappa_w = \frac{k_f}{k}$
1	37.5	7.5	2	.2	.266
2	37.5	15	2	.4	.133
3	37.5	30	2	.8	.067

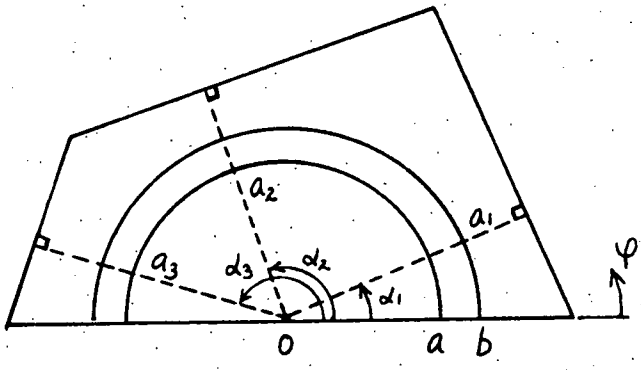

Fig. 1 Configuration of a Unit Cell

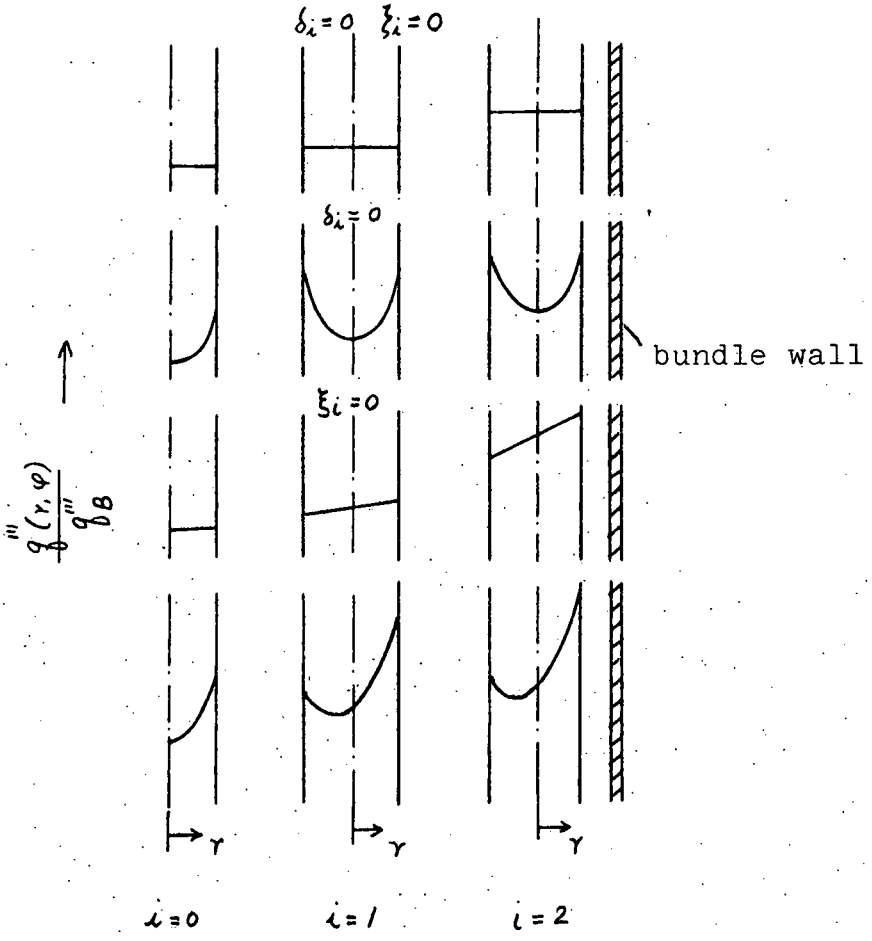

Fig. 2 Simulation of Different Power Densities

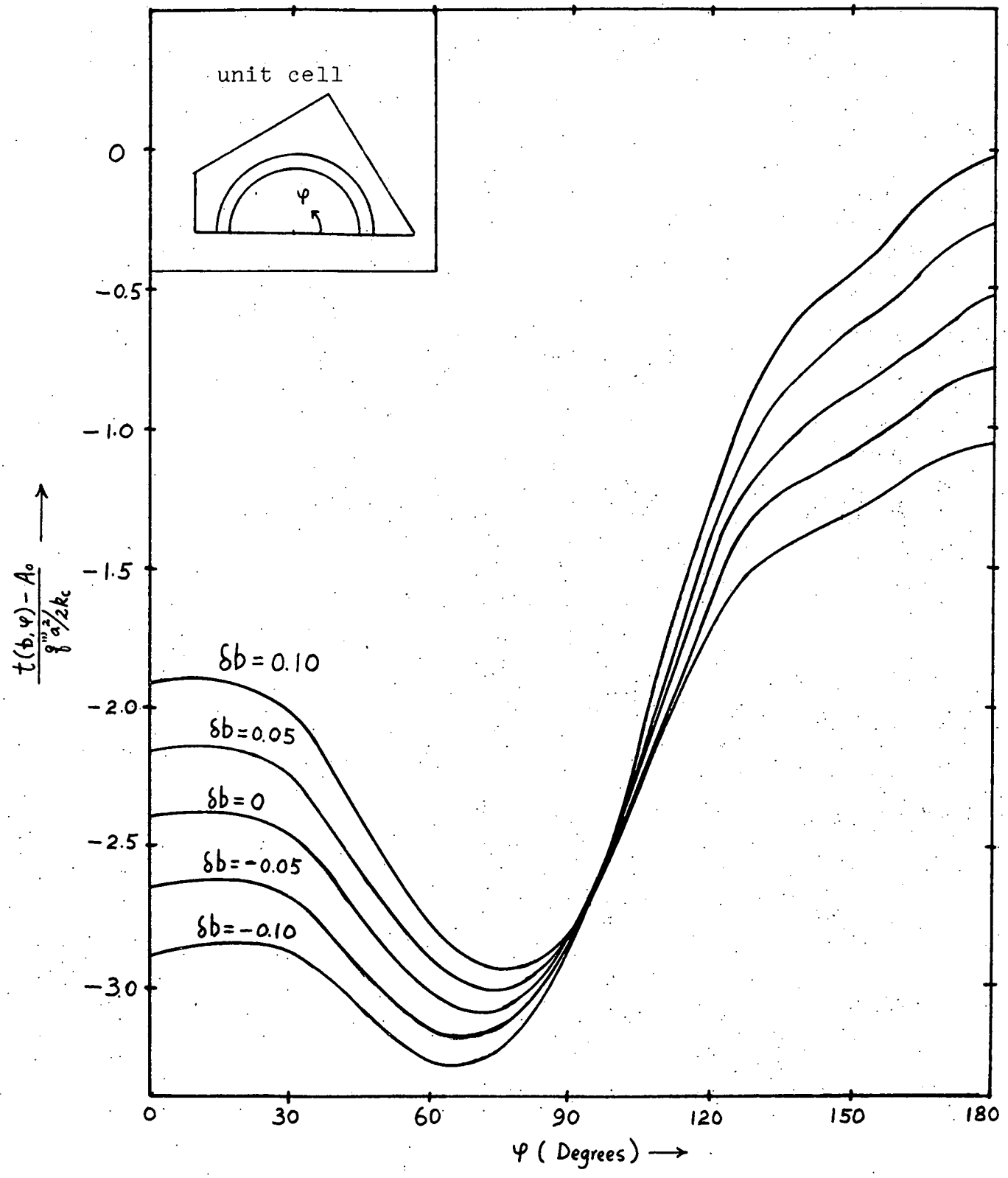

Fig. 3 Dimensionless Clad Outside Temperature Distributions of the Corner Cell

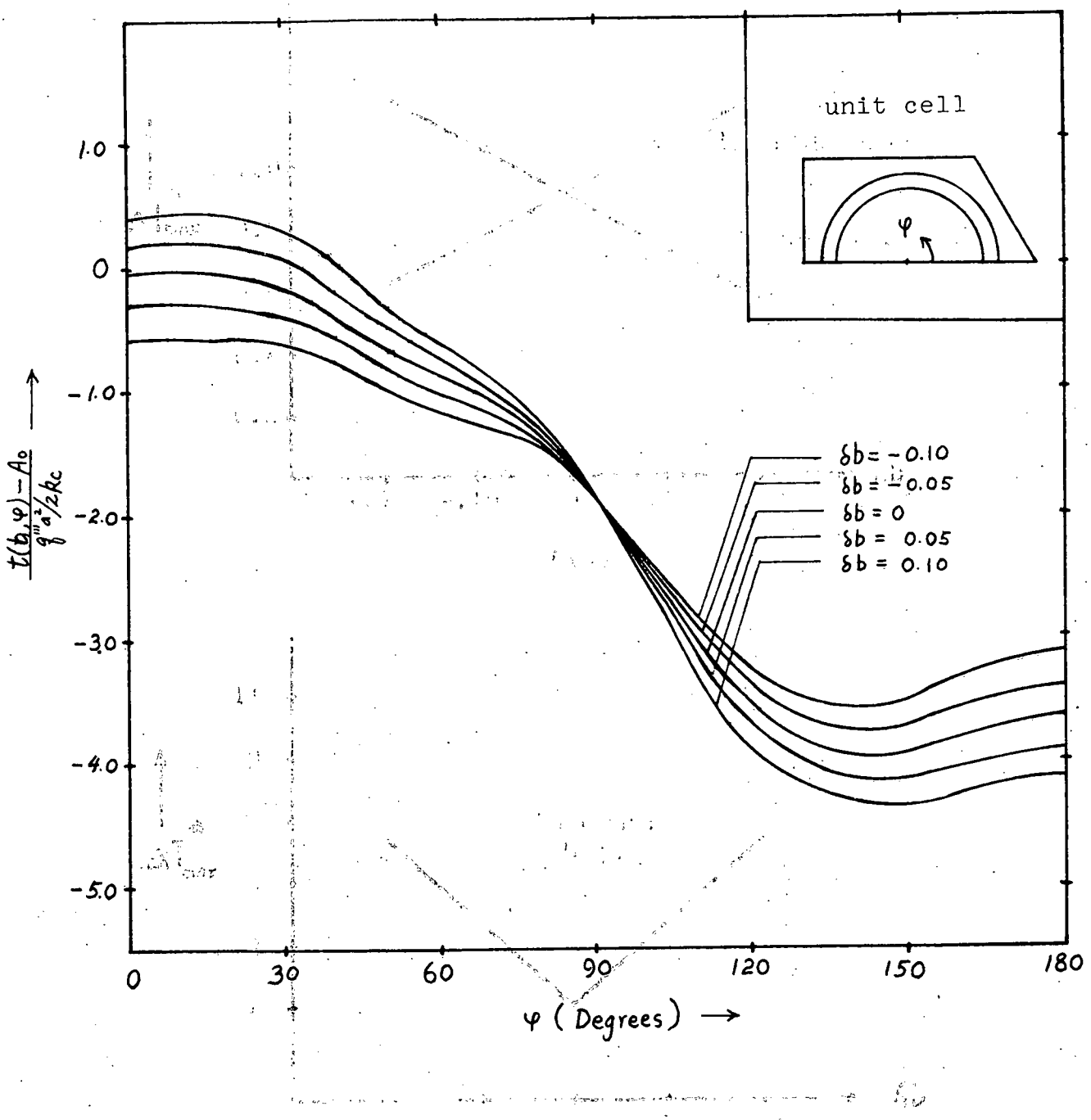

Fig. 4 Dimensionless Clad Outside Temperature Distributions of the Edge Cell

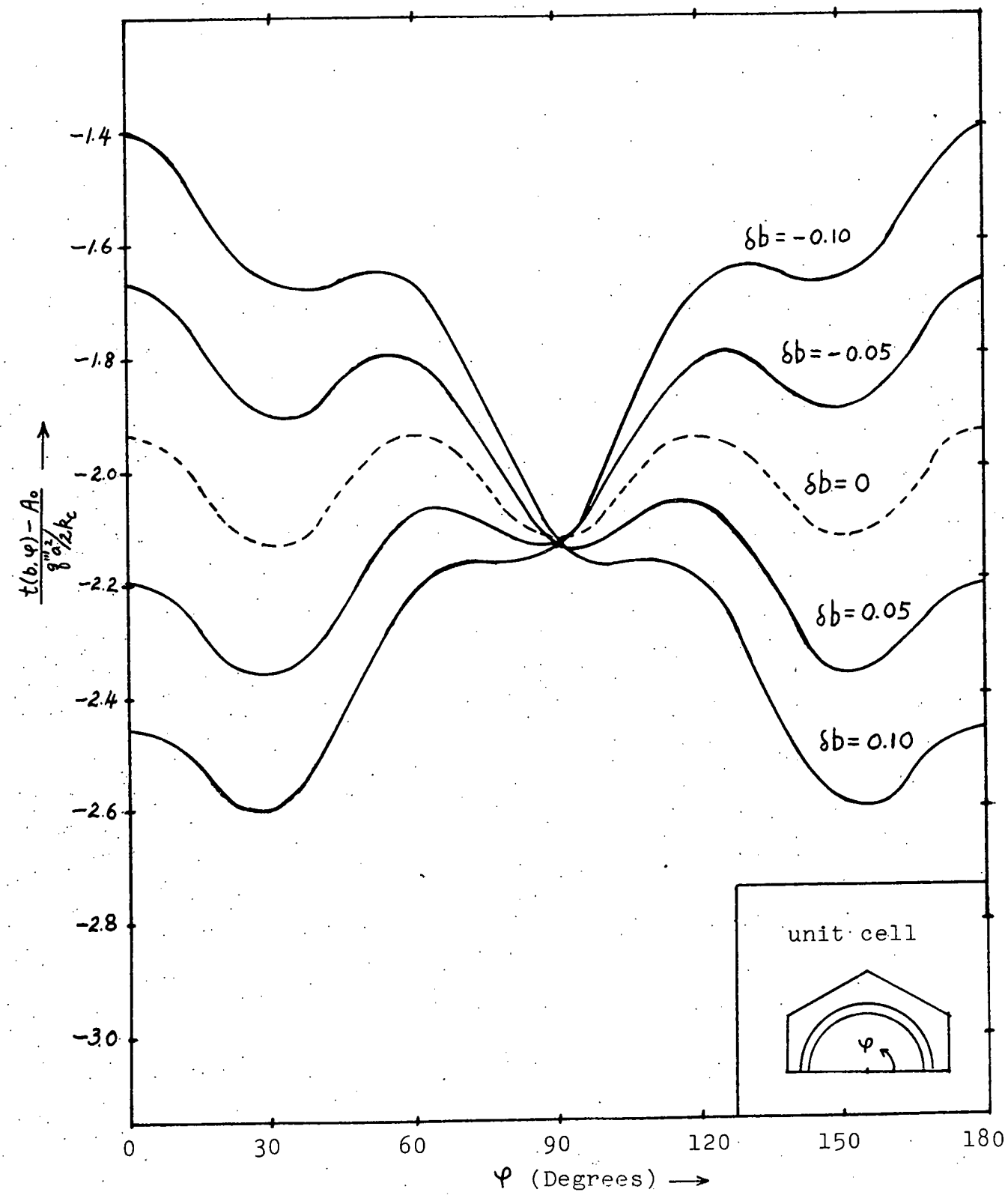

Fig. 5 Dimensionless Clad Outside Temperature Distributions of the Internal Cell

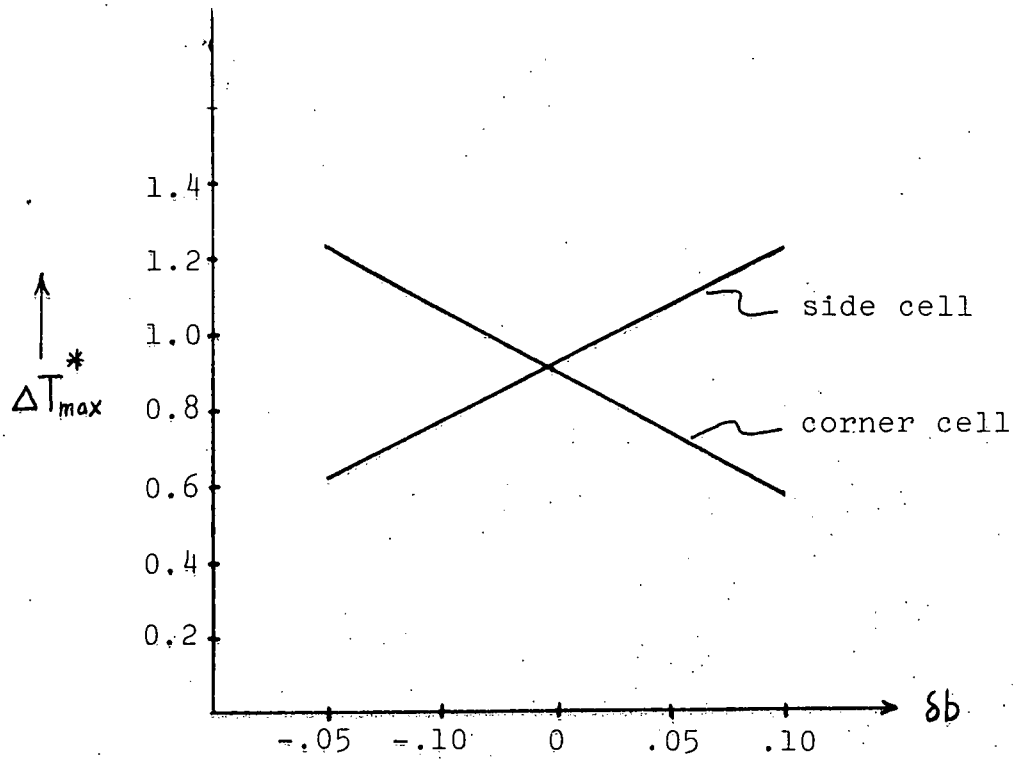

6(a)

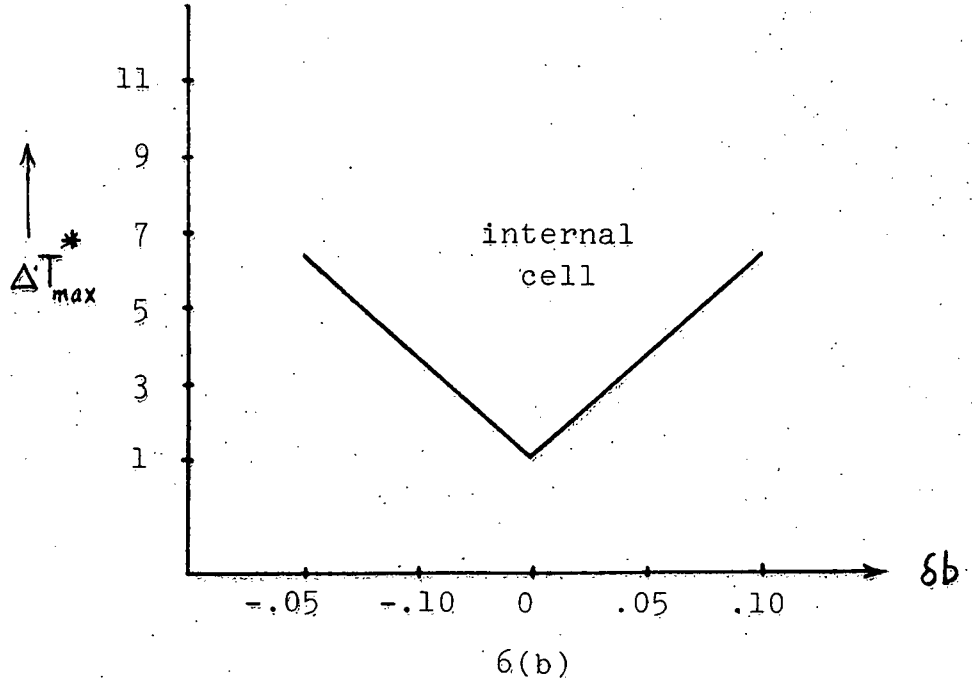

6(b)

Fig. 6 Circumferential Clad Outside Temperature Variations as a Function of Power Tilting Parameter

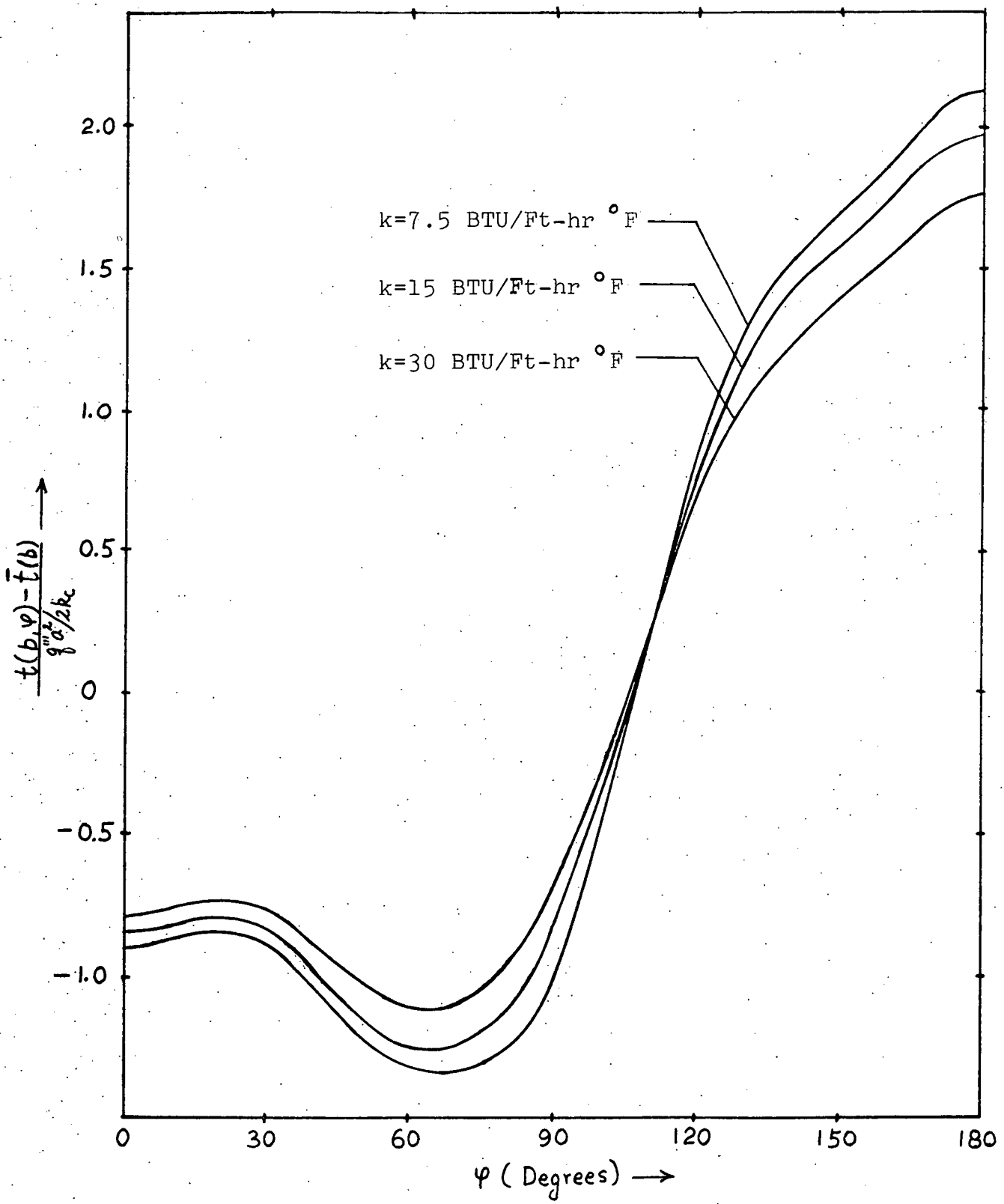

Fig. 7 Clad Outside Temperature Distributions of Corner Cell with Different Clad Thermal Conductivities

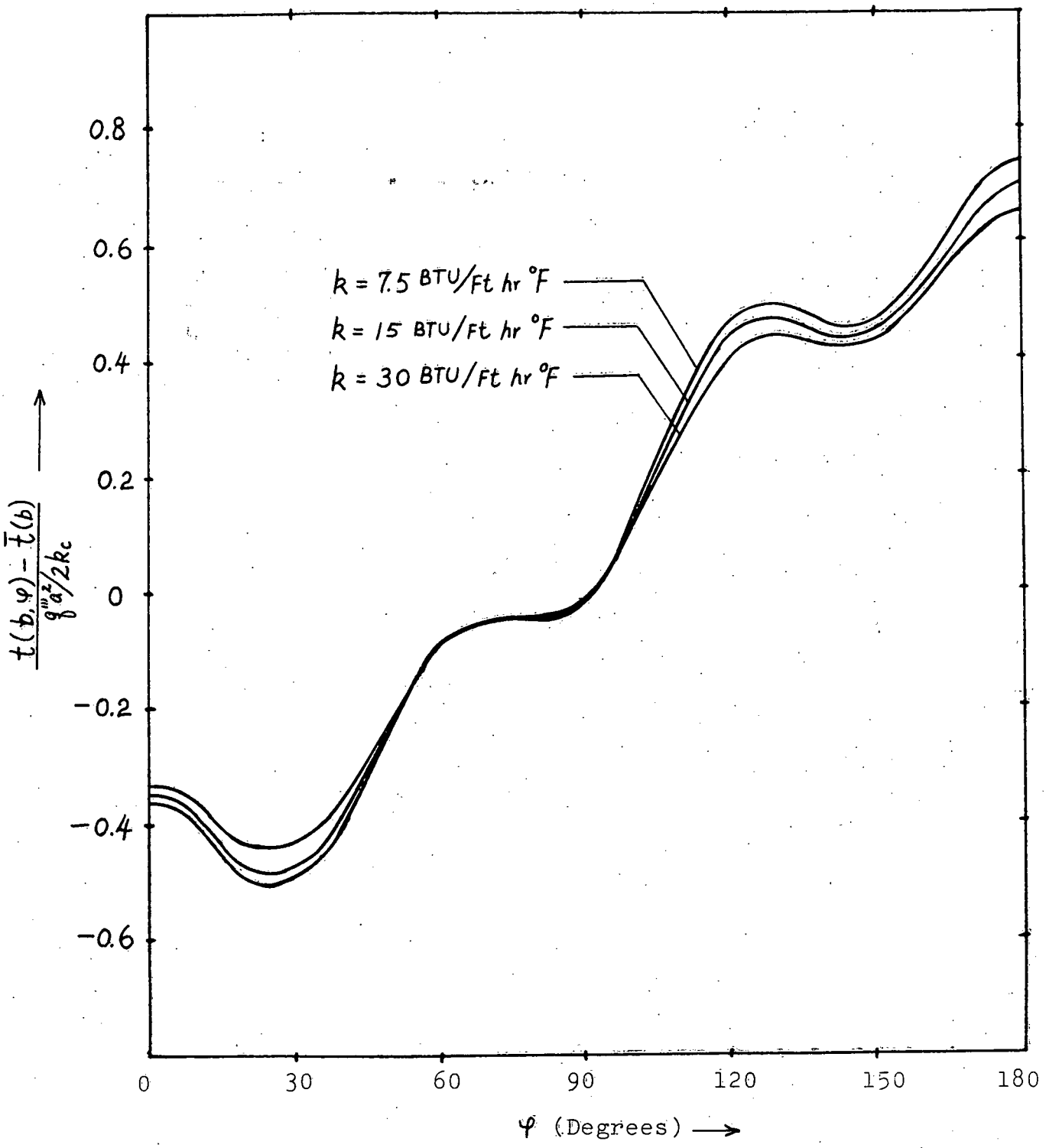

Fig. 8 Clad Outside Temperature Distributions of 4-side Internal Cell with Different Clad Thermal Conductivities

Figure 9. Clad Temperature Distribution of Fuel Element of Clinch River Breeder Reactor

—— coupled (non-uniform heat flux)

- - - - isolated (non-uniform heat flux)

Conditions:

P/D = 1.24 2W/D = 1.42

D = 0.23" H = 36"

T_{inlet} = 730°F

Pe = 357

q' = 6.67 KW/ft.

Peaking Factor = 1.24

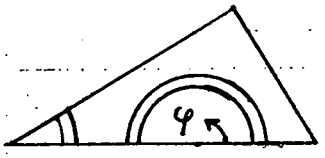

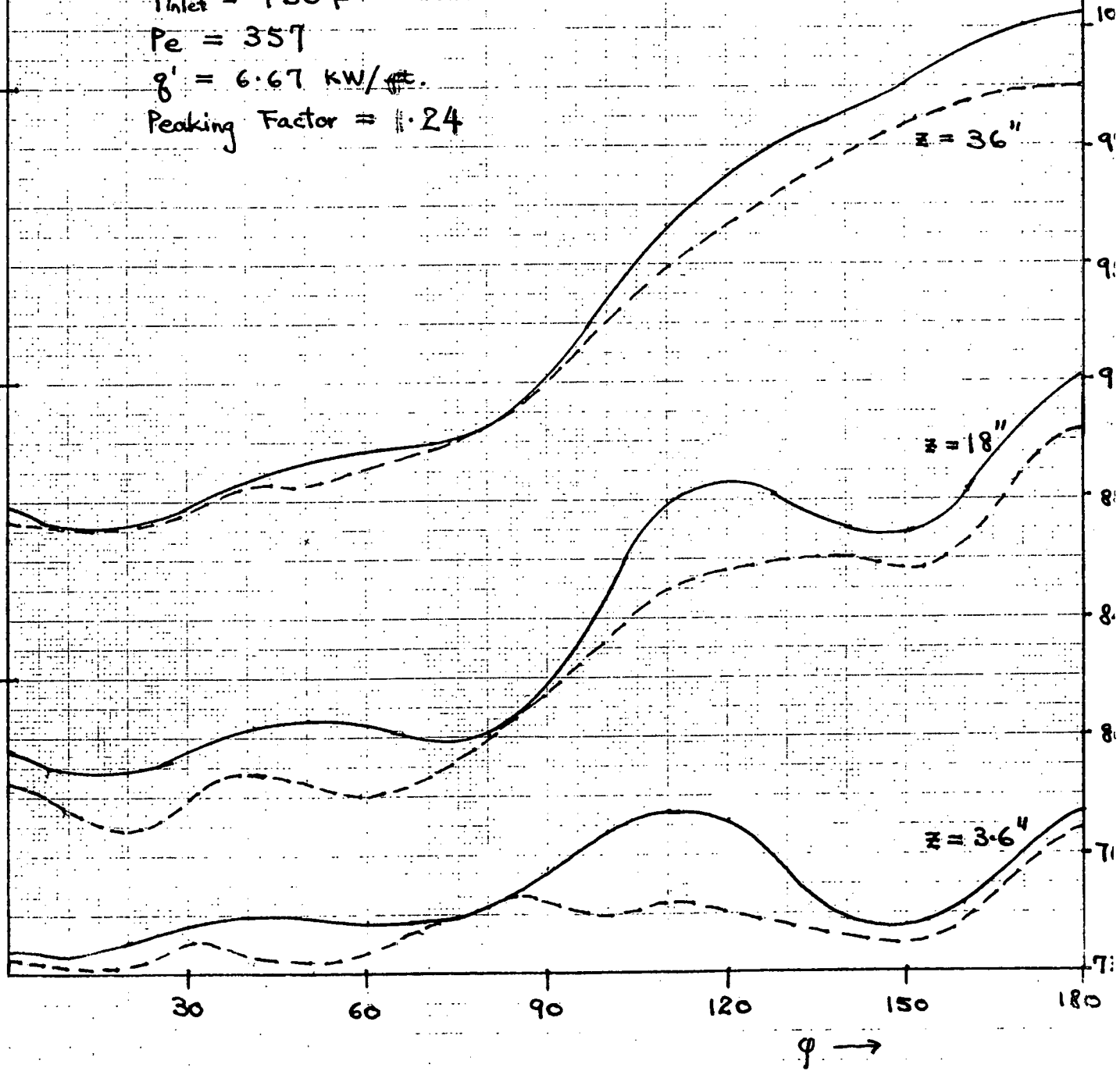

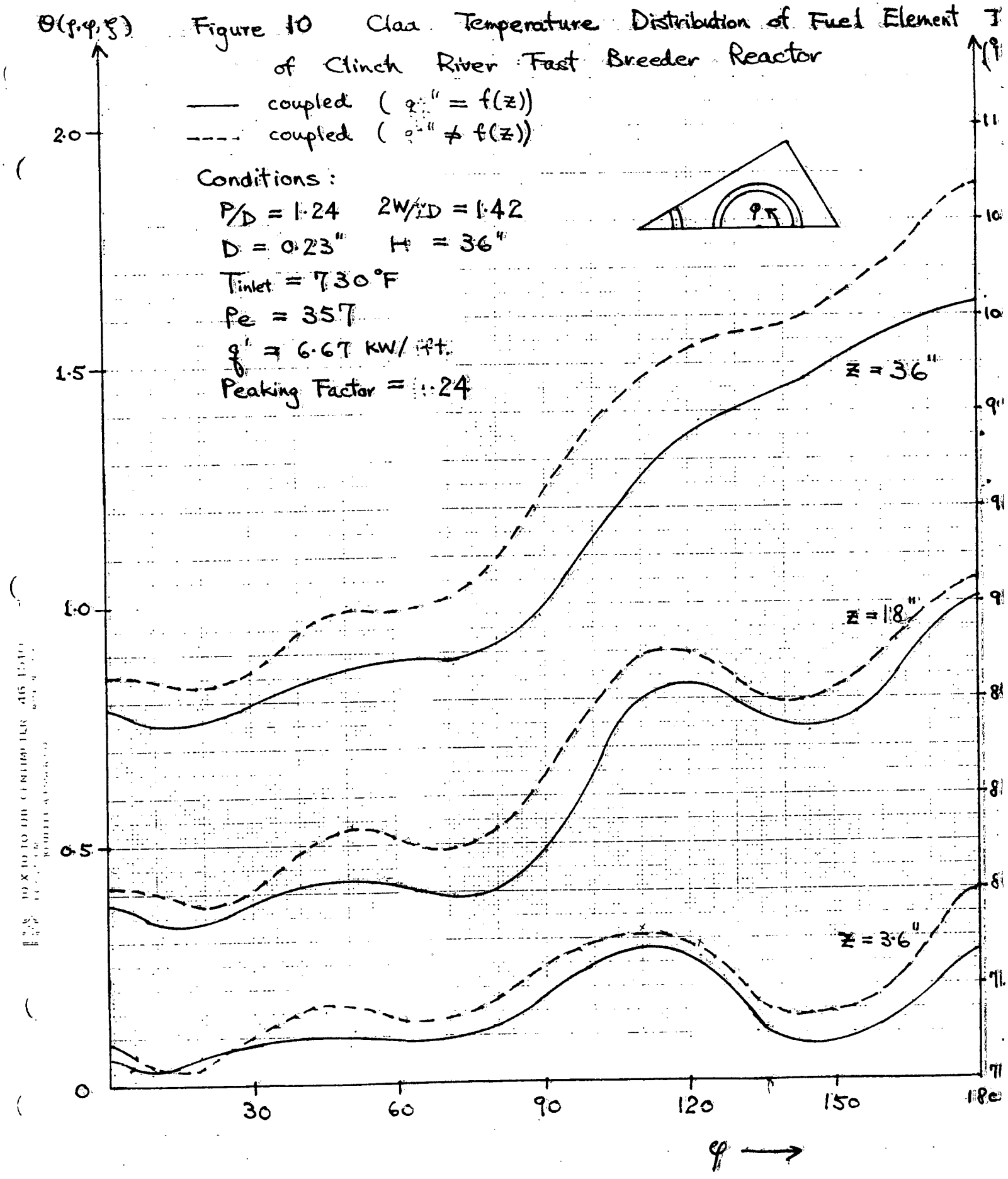
Θ(ξ,φ,ξ)
Figure 10 Clad Temperature Distribution of Fuel Element
of Clinch River Fast Breeder Reactor
coupled ($q''' = f(z)$)
coupled ($q''' \neq f(z)$)
Conditions :
P/D = 1.24 2W/D = 1.42
D = 0.23" H = 36"
Tinlet = 730°F
Pe = 357
q' = 6.67 KW/ft.
Peaking Factor = 1.24
z = 36"
z = 18"
z = 3.6"
2.0
1.5
1.0
0.5
0
30
60
90
120
150
180
φ

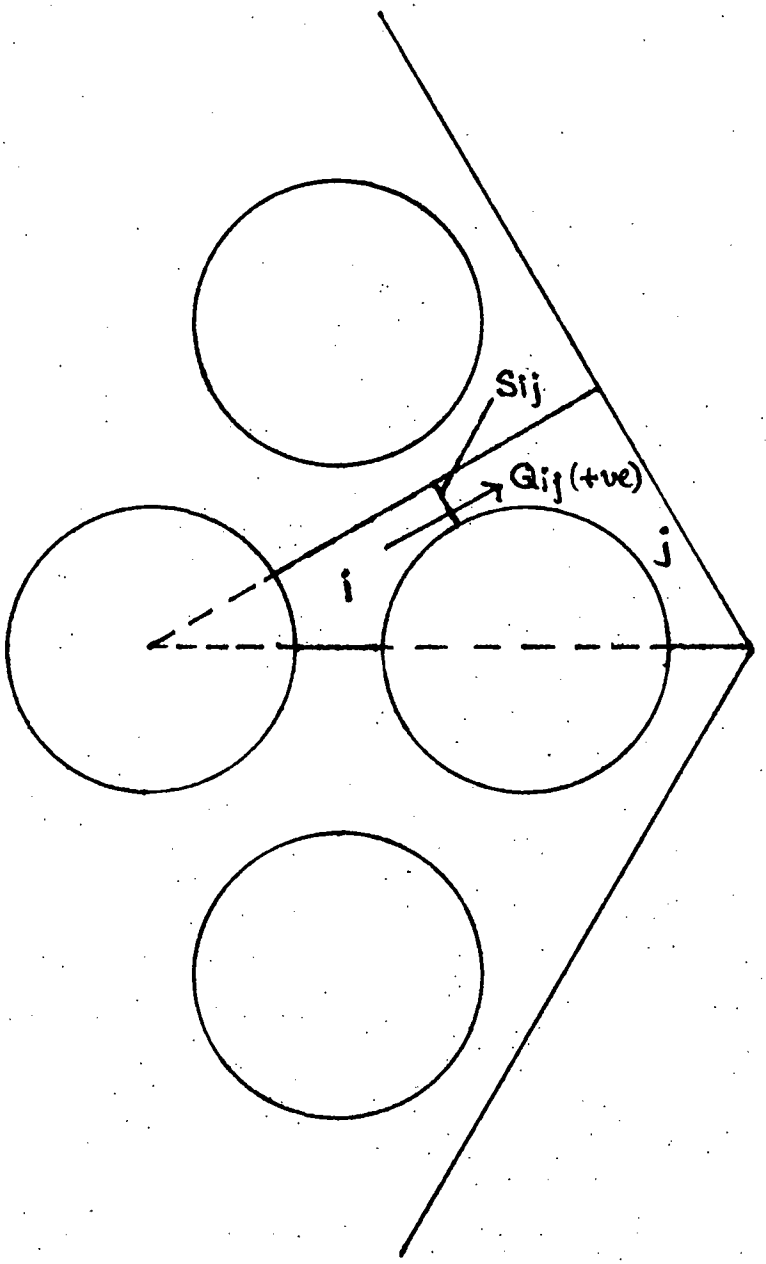

Figure 11 Diagram illustrating subchannel i and subchannel j.

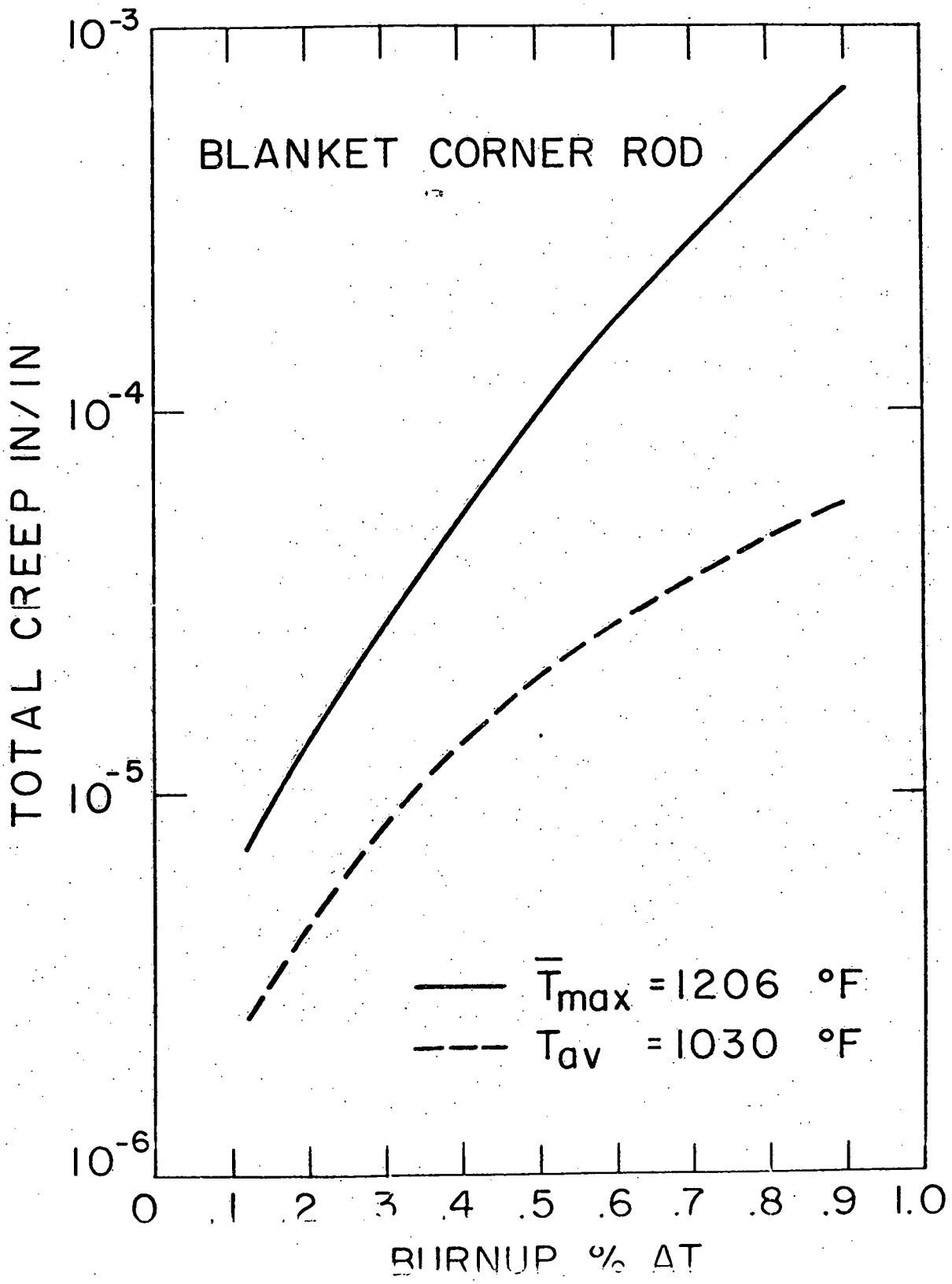

Fig. 12. Total Clad Creep (Thermal, Irradiation, Swelling) as Function of Burnup for a Blanket Corner Rod with Average and Maximum Temperature Loads (Material: 20% CW 316 SS)

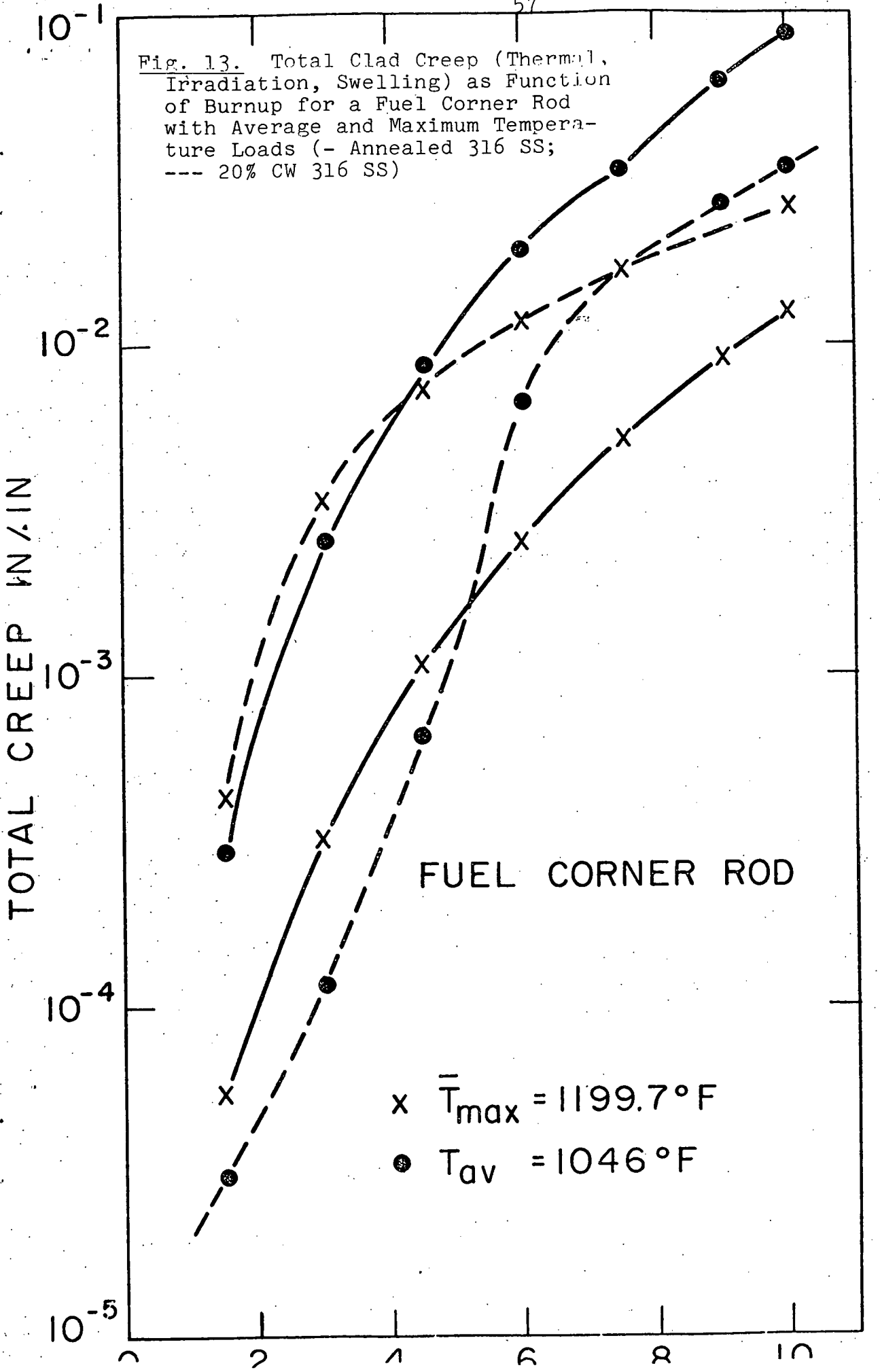

Fig. 13. Total Clad Creep (Thermal, Irradiation, Swelling) as Function of Burnup for a Fuel Corner Rod with Average and Maximum Temperature Loads (- Annealed 316 SS; --- 20% CW 316 SS)